CHALMERS
UNIVERSITY OF TECHNOLOGY

Master's Thesis

Reduction of Crosstalk Distortion in 5G

Relaxed Isolation based Linearization for sub-6 GHz Advanced Antenna Systems

By

Ali Al-Qamaji and Fida Abdalrahman

Department of Electrical and Information Technology
Faculty of Engineering, LTH, Lund University
SE-221 00 Lund, Sweden

Wireless, Photonics and, Space Engineering Master Program
Department of Microtechnology and Nanoscience
Chalmers University of Technology, Gothenburg, Sweden

2019

Abstract

Increasing demand for higher data rates in wireless communication systems has tremendously evolved over the last years. This demand is rapidly increasing with rising in number of wireless devices. Advanced antenna systems (AAS) – known as massive MIMO – is one of the central enabling radio technologies for 5G cellular systems that significantly increase the data rates provided for data-hungry applications.

A fundamental component in the realization of multiple antenna systems is the radio frequency (RF) power amplifier (PA) at each transmitter branch. The reason for its crucial role is because it takes the responsibility of amplifying the transmitted signal to suitable power levels for transmission. These RF PAs are the most power-hungry components in RF transmitters. Consequently, their energy efficiency is a major concern. One way to increase the PA efficiency is by increasing the input signal power to the PA. However, the signals, using modern modulation schemes, e.g., Orthogonal Frequency Division Multiplexing (OFDM) and Wideband Code Division Multiple Access (W-CDMA), have high Peak to average power ratio (PAPR). Hence, PAs introduce nonlinear distortion to the amplified signal. This nonlinear behavior of PAs does not only distorts the transmitted signal (in-band distortion), but also produces spectral regrowth which causes interference to the other signals in neighboring channels (out-band distortion). Due to these distortions, 3GPP spectrum regulations might be violated in terms of in-band and out-band distortions. Hence, PAs are required to be linear and highly efficient. To do so, some linearization technique can be used, like Digital Pre-distortion (DPD) to linearize the PA behavior.

Massive MIMO systems contains up to several hundreds of antennas, and these antennas are closely attached. This complicates the transmitter structure, and the smaller space between antenna elements increases the cross-talk between them due to mutual coupling. In addition to that, there is impedance mismatch between the power amplifier and the antenna at each radio branch. As a consequence, these multiple antenna systems are suffered from nonlinear distortion due to the combining effects of mismatch and cross-talk at the output of PA, in addition to the non-linear distortion from PA itself at high PAPR. To avoid both mismatch and cross-talk coupling effects, expensive and bulky isolators should be placed between PAs and antennas, which increase system design complexity and cost. Hence, the project main aim is to relax the isolation requirement, while applying linearization technique (DPD), to save the cost, complexity and reduce the design requirements in base stations.

In this project, the DPD is implemented as a linearization technique, using a behavioral model of PA that counts for PA non-linearity and cross-talk, while mismatch effects is not considered. Further investigations are carried out to test different levels of isolation to know up to which extent the isolation can be relaxed while keeping the Adjacent Channel Leakage Ratio (ACLR) level of -50 dBc, due to 3GPP regulations. These investigations led to a conclusion that, in sub-6 GHz, it would be impossible to relax the isolation level if the PA model that does not count for cross-talk coupling is used. In contrast, when counting for cross-talk coupling in the PA behavioral model, isolation level is relaxed to about 11 dB while keeping the targeted ACLR level.

Acknowledgements

We would like to express our gratitude and thanks to everyone who helped us to finish this work.

First of all, a great thank goes to all people at Ericsson AB, Lund. To Our main supervisor at Ericsson, Mohamed Hamid, for his unlimited guidance and support. To Hans Hagberg and Christian Elgaard for generating many signals and simulations for us and for their unlimited help, they offered during the project.

Special thanks go to Our supervisors and examiners at Lund University and Chalmers University of Technology, Christian Fager, Ove Edfors, Linag Liu and Fredrik Rusek, for their great help and supervision while working on this project.

To our dear friends and colleagues in Sudan,Turkey, Iraq, Sweden and all over the world for their unlimited encouragement during our study at Sweden.

Nothing can express our gratitude to our kind parents, our brother and sisters. This journey would be impossible without their support.

Lund, Sweden

Ali AL-QAMAJI and Fida ABDALRAHMAN

Table of Contents

List of Figures

Abbreviations and Notations

Abbreviations

3GPP 3rd Generation Partnership Project

5G the 5th Generation in communication

AAS Advanced Antenna System

ACLR Adjacent Leakage Ratio

ADC Analog to Digital Converter

BER Bit Error Rate

BJT Bipolar Junction Transistor

D2D Device-to-Device

DAC Digital to Analog Converter

DPD Digital Predistortion

DUT Device Under Test

EVM Error Vector Magnitude

HPA High Power Amplifiers

HFET Heterojunction Field Effect Transistor

ILA Indirect Learning Architecture

IoT Internet of things

LNA Low Noise Amplifier

LO Local Oscillator

MESFET Metal-Semiconductor Field Effect Transistor

MIMO Multiple Input Multiple Output

MISO Multiple Input Single Output

MP Memory Polynomial

MMICs Microwave Monolithic Integrated Circuit is

MOSFET Metal Oxide Semiconductor Field Effect Transistor

NMSE Normalized Mean Squared Error

NR New Radio

OFDM Orthogonal Frequency-Division Multiplexing

PA Power Amplifier

PAE Power Added Efficiency

RF Radio Frequency

Notations

η ; power amplifier efficiency

P_{out} ; RF output power from PA

P_{DC} ; DC power supply

P_{in} ; RF input power

G_v ; voltage gain

M ; memory depth

P ; non-linear order

$\boldsymbol{a_1}$; direct PA input

$\boldsymbol{a_2}$; indirect PA input

$\boldsymbol{b_2}$; output from PA

Popular Science Summary

The demand for better and faster service, data-rates increases every day to satisfy different users' requirements, and the limits of wireless networks become more visible. Studies have shown that in 5G generation, data rates up to tens of Gigabit per second (Gbit/s) can be achieved. Multiple Input Multiple Output (MIMO) system is one of the promising solutions for LTE (4G) and 5G wireless communication, by using multiple antennas in the transmitter and receiver, to achieve better reliability and higher data rates.

Power amplifiers (PAs) are important components in multiple antenna systems for amplifying the transmitting signal to be detectable and receivable at the receiver end. The PAs must only amplify transmitting signal linearly, the power level of the amplified signal is a scaled version of input power level. However, due to modern modulation schemes, the signals might have high power level, hence PA behaves non-linearly. In addition, for multiple antenna systems, with a large number of antennas of closely-spaced, a part of transmitting signals after PA is leaked from one antenna to other antenna, i.e., crosstalk, which distorts the amplified signal. Due to that, PA distorts the signal within the desired communication bandwidth (in-band) and generates out-of-band signals that interfere with the transmitting signals from neighboring users.

The motivation, in this thesis, is to improve the PA performance to act linearly. This can be addressed by using isolators for cross talk. However, they can introduce losses and they are bulky and expensive, also, they take relatively large space in 5G base stations. This means, there is a necessity for a robust and less-complicated algorithm to compensate for coupling effects in the 5G system.

The main aim of this thesis is to compensate for these combined nonlinearity effects of PA, including cross-talk, at output in MIMO transmitters using Digital Pre-distortion to minimize the isolation requirements at 5G base stations.

1

Introduction

Wireless communication is the transfer of data between two or more points by using radio waves. Wireless communication allows users to communicate remotely using modern technologies such as cellular networks, Wi-Fi, satellite communication links, Bluetooth, etc. The RF signals are commonly used in modern wireless communication systems to serve several users as well as enable a wide range of applications [1].

Over the past few years, day-to-day lives were transformed through the Internet of things (IoT) connected devices, sensor nodes, and other parallel devices. It is obvious that, the wireless communications will experience huge demands for a higher date as well as the more advanced wireless solutions to support these massive requirements. Modern wireless communication standards like LTE and 5G is employed for data-hungry applications. To meet the requirements of higher data rate, the wireless communication system cannot only rely on bandwidth, as the frequency spectrum is getting crowded and more expensive. For this, researching in the field of multiple antenna systems takes a significant role in the modern wireless communication system.

Multiple Input Multiple Output (MIMO) [4] systems have already become a crucial part of current wireless communication standards like LTE and 5G. MIMO technology has led to Advanced antenna systems (AAS) that also known as Massive MIMO. These multiple antenna systems are employed to provide higher data rates, more capacity and better link reliability. They reduce link failure probability by exploiting spatial diversity.

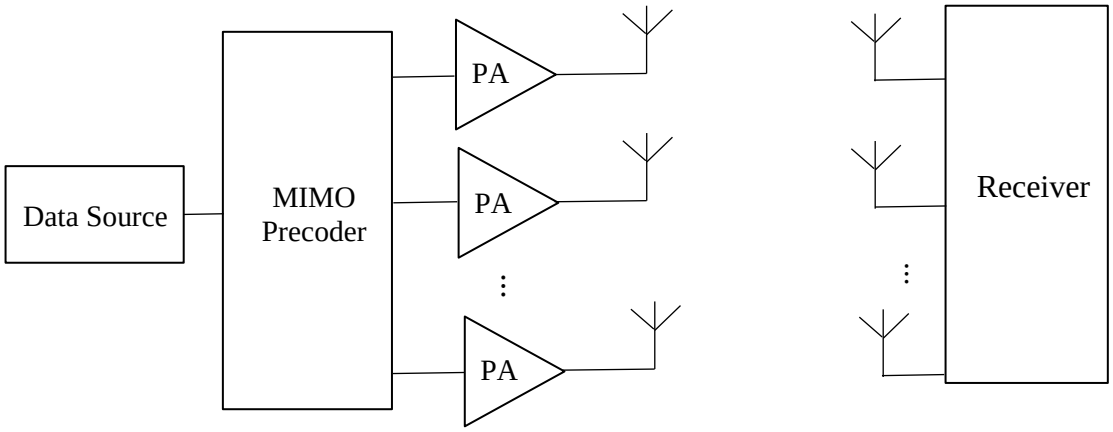

Figure 1: Multiple Input Multiple Output (MIMO)

Excessive energy consumption of information and communications technology (ICT) is a growing concern these days. One study suggests that by 2020, 11% of the world's total energy output will be consumed by ICT. Furthermore, as much as 90% of energy consumption in cellular systems is consumed in base stations and their related hardware [2] [3]. In base stations, the most consuming component is the PAs. Hence, it is always a challenge to increase the energy efficiency of PAs, which is can be increased by increasing the input power. However, in current cellular systems like LTE and 5G, advance modulation techniques are used, e.g., Orthogonal Frequency Division Multiplexing (OFDM), which it has high peak to average power ratio (PAPR). Due to high PAPR, PA might behave nonlinearly. In such a case, a spectrum regrowth is detected for the amplified signal, that results in the violation of 3GPP standards, which define the maximum acceptable Adjacent Channel Leakage Ratio (ACLR) for the mobile communications standards e.g. LTE (4G) and 5G.

In this introductory chapter, the basic building blocks of radio communication link are presented, some enabling techniques in 5G are also illustrated. The motivation and main objectives of this project are briefly described.

1.1 RF Wireless Link

A wireless communication link can be constructed by a transmitter and a receiver, as shown in Figure 2. A typical radio transmitter, Figure 2 (a), consists of a digital to analog converter (DAC) that converts the digital data to an analog signal to be modulated to the carrier frequency. In the modulation process, the signal is upconverted by the mixer into a specific carrier frequency which is generated by the local oscillator (LO). A power amplifier (PA) is then used to amplify the modulated signal before radiating it into free space by the antenna. Isolators[1] can be used to protect the PA from any reflected wave due to the mismatch between the PA and antenna.

In the receiver part, Figure 2 (b), the antenna receives different signals from the space, and not all these signals are desired, hence, the desired frequency band is selected using a bandpass filter (BPF). This very low and attenuated signal must be amplified using a Low Noise Amplifier (LNA). Later, the signal is down converted to baseband frequency. A band pass filter (BPF) is also used to select the desired frequency channel before demodulating the signal in digital domain.

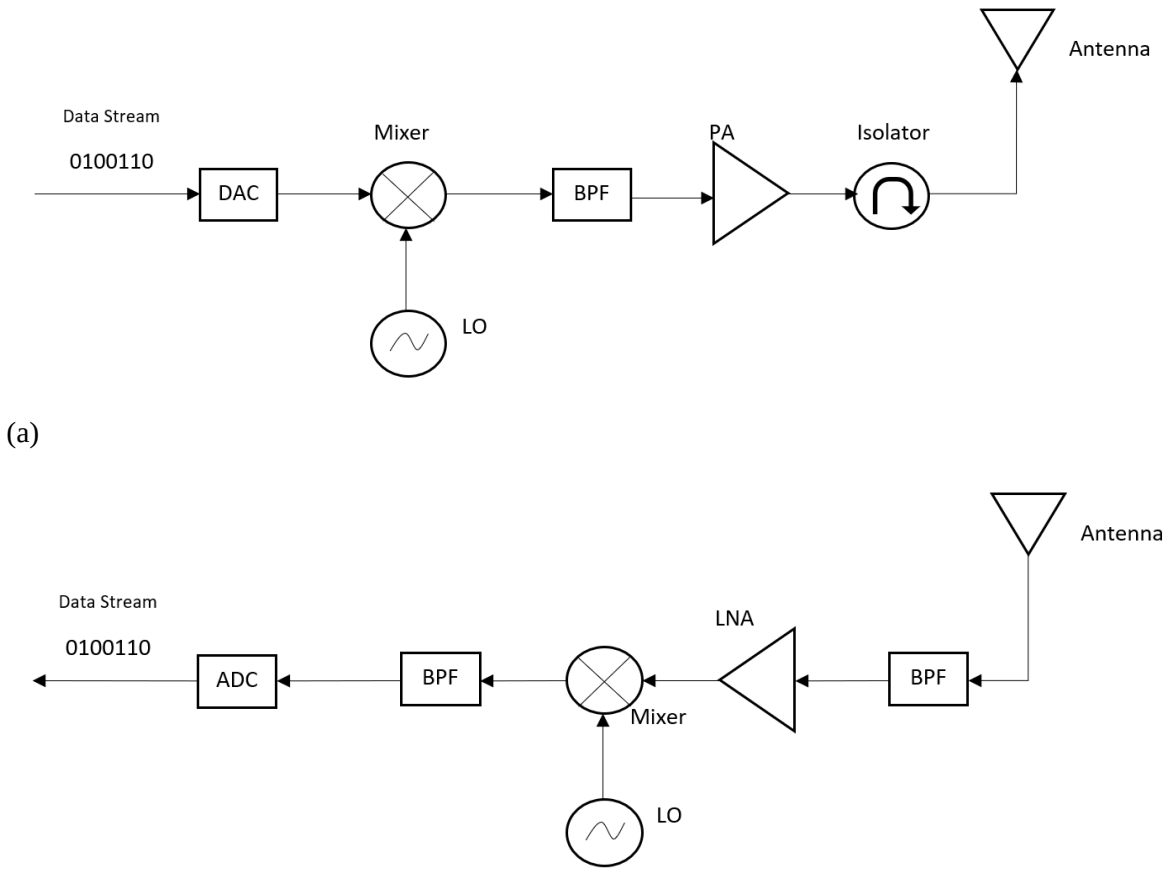

Figure 2: Block diagram of a basic radio system: (a) transmitter, (b) receiver

1.2 Beamforming and MIMO Hardware

Beamforming is one of potential techniques that have been used to enable 5G in Massive MIMO (AAS) systems. In general, beamforming uses multiple antennas to control the direction of the

[1] Detailed description of circulators and isolators can be found in Appendix 9.2.

transmitting signal by adjusting the magnitude and phase for each antenna signal in multiple antenna array. In beamforming, the same signals are fed to these antenna arrays, and the antennas have appropriate space between them (about ½ wavelength). The receiver end will receive multiple copies of the same transmitted signal. Depending on the receiver location, these signals may be in opposite phases, destructively canceling each other, or in same phase, constructively sum up, or anything in between. The PA is a circuit that uses a DC power supply to increase the power level of the input signal [5] at each branch. The phase of the beam can be changed either by connecting a phase shifter prior to each PA (analog beamforming) or by producing different signals with different phases for each antenna element (digital beamforming), as in Figure 3 [6]. In analog beamforming, only one beam is created for the entire frequency band. In contrast, in digital beamforming, many beams can be created [7]. In this project, the considered scenario is digital beamforming.

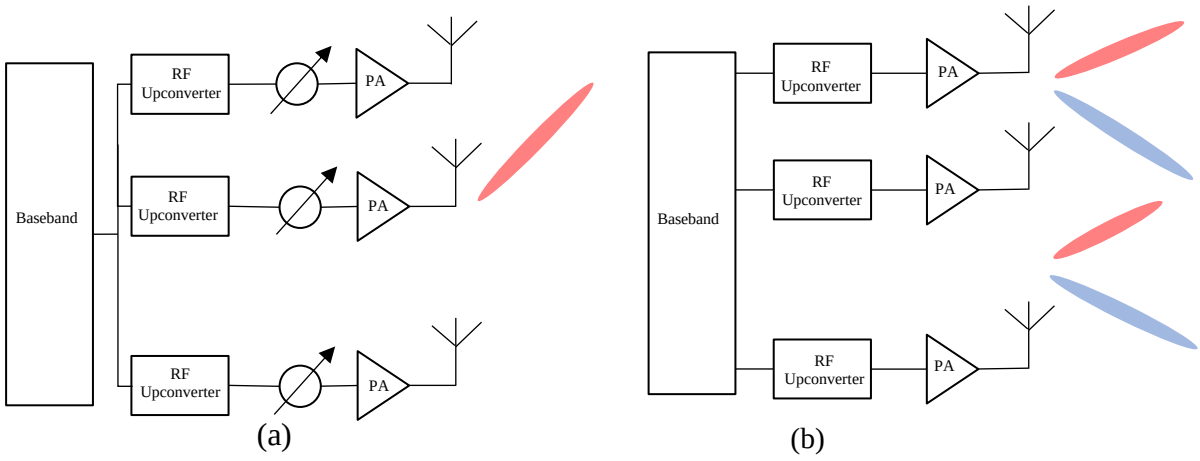

Figure 3: Beamforming; (a): Analog beamforming, (b): Digital beamforming

Moving up in frequency means scaling down in wavelength and hence, in dimensions of antenna array. For instance, the patch dimensions in 27 GHz frequency is approximately (2.2x3.1) mm^2 [8], in compare with (36.5x47) mm^2 when operating at 1.9 GHz [9]. Accordingly, in the upper microwave and millimeter wave regions, the antenna size will be smaller in terms of wavelength. In such high-frequency regions, the active modules, i.e. PAs is integrated with the antennas on the same chip. Hence, microwave monolithic integrated circuit is (MMICs) can also be considered in order to reduce the size and the cost of manufacturing modules in large numbers.

Using such integrated modules means that it is difficult and even, sometimes, impossible to insert bulky isolators between the PA and the antenna. Hence, it is essential to find a way to solve the distortion that may be caused due to crosstalk, instead of using these expensive and bulky isolators, or at least to find a method to relax the isolation level of these isolators.

1.3 Background and Motivation (problem outline)

In MIMO transmitter design, nonlinearity is a big issue. It is mainly introduced by the nonlinear behavior of RF PAs and by the cross talk (coupling) through interaction between branches in antenna array. As a result, this leads to power leakage into adjacent channels, and this leakage should be kept under a certain level. For sub-6 GHz transmitters, the accepted Adjacent Chanel Leakage Ratio (ACLR) level has been specified in 3GPP requirements to be -45 dBc [26]. The distortion caused by cross talk and mismatch can be reduced using high quality and expensive isolators. However, these isolators are bulky, lossy, and it is expensive to integrate them in radio branches.

New technology has been recently suggested and implemented to compensate for these effects of PA non-linearity and crosstalk coupling effects. That is done by implementing linearization techniques, known as MIMO based digital pre-distortion (MIMO DPD). By using MIMO DPD algorithm, is it possible to relax the isolation requirements with respect to 3GPP standards?, if so to which level can be

relaxed? And what is the minimum complexity for MIMO DPD, in terms of the memory depth and nonlinear order?

1.4 Objectives

The main objectives of this master's thesis work are listed below:

- Analyze power amplifier (PA) characteristics and nonlinear behavior using Dual-input simulations, that consider the direct input signal and the cross-talk signal. The simulations are based on sub 6 GHz AAS systems.
- Modeling the nonlinear behavior of PA using dual-input Memory Polynomial (MP) and test the model accuracy, by comparing the actual output with the modeled output.
- Study DPD algorithms and examine DPD performance without cross-talk signal (SISO DPD) and with crosstalk signal (MIMO DPD).
- Study DPD algorithms and investigate DPD performance for different isolation levels. This is done by executing DPD algorithm for different isolation level and measuring the resulted in-band and out-of-band distortions.
- Select minimum isolation level with minimum complexity for DPD in terms of memory depth and nonlinear order, with respect to 3GPP requirements on both in-band and out-of-band distortions (ACLR =-45 dBc).

1.5 Thesis Outline

This introductory chapter is followed by six chapters. In the second chapter, the main concepts of PA functionality, classes, efficiency, gain compression and memory effects are illustrated. Chapter three, presents the idea behind PA modeling and model parameters extraction approach. Some common linearization techniques are presented in the fourth chapter, the digital pre-distortion will further be illustrated as the main technique used in this project. Implementation methodology will be described in detail in the fifth chapter, while the corresponding results will be presented and discussed in chapter six. The project conclusion and some proposed future enhancement will be highlighted in the seventh chapter.

2

Power Amplifier Characterization

In order to study the behavior of PA, a detailed description of its features, operating classes, efficiency, non-linearity and memory effects will be presented in this chapter.

2.1 Power Amplifier functionality

Power amplifiers can be considered as one of the most important components in the radio transmitter chain. The generated signal is fundamentally weak in terms of power and it needs to be amplified to overcome the loss in the transmission or channel path between the transmitter and receiver. Power amplifiers are non-linear devices, which means that their output power does not always increase linearly in proportion to the input power. This non-linearity is distorting the signal and introduces in- and out of band distortions that are further discussed in the following sub-sections.

2.2 Efficiency of Power Amplifiers

Radio transmitter contains several parts that work together to generate radio waves that contain the intended information. Among all these parts, power amplifier has the highest power consumption. They can consume up to *40%* of the overall power budget [11]. That makes it very challenging for engineers to design high-efficient power amplifiers, to keep an acceptable tradeoff between consuming DC power and output power levels.

The efficiency of PA is a measure of its ability to increase the output power, P_{out}, of RF signal after supplying direct current (DC) power from the DC source, P_{DC}, as an input. The efficiency can be defined in two methods. It can be either defined in terms of drain efficiency (η), as in (1), or power added efficiency (PAE) that it is more commonly used, as in (2).

$$\eta = \frac{P_{out}}{P_{DC}} \tag{1}$$

$$PAE = \frac{P_{out} - P_{in}}{P_{DC}} \tag{2}$$

where P_{in} is the RF input power.

2.3 Power Amplifier Classes

RF PA, Figure 4, consists of a transistor (MOSFET, MESFET, HFET, or BJT), input and output networks [5]. RF PAs are classified depending on the conduction angle of the drain current and their efficiency. Four classes of PA are commonly used in analog design; class A, B, AB and C. In class A, the conduction angle, as in Figure 5 (a), of the drain current is 360°, this means the transistor is 'ON' during the entire cycle. Hence, it has lower efficiency (*50%*) but linear behavior. Class B, Figure 5 (b), has a conduction angle of 180°, which means it conducts only half of the cycle. Meanwhile, it has higher efficiency than class A (about *78.5%)*.

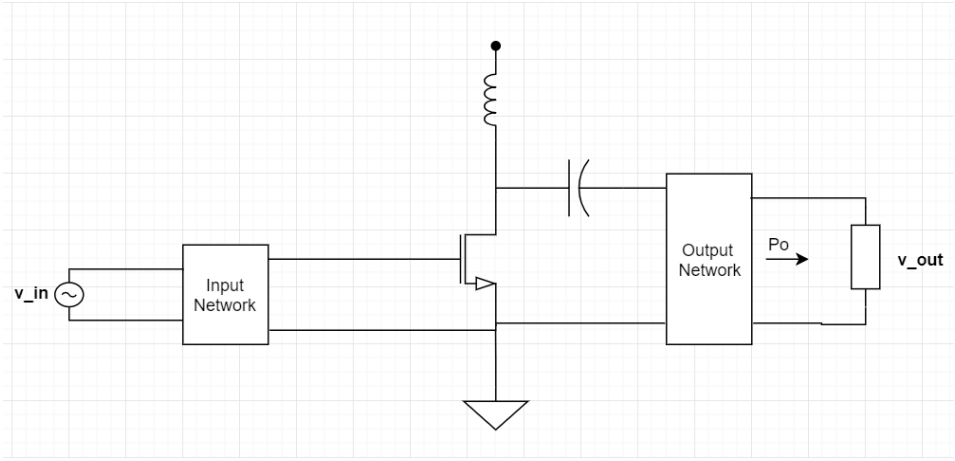

Figure 4: Radio frequency power amplifier basic scheme

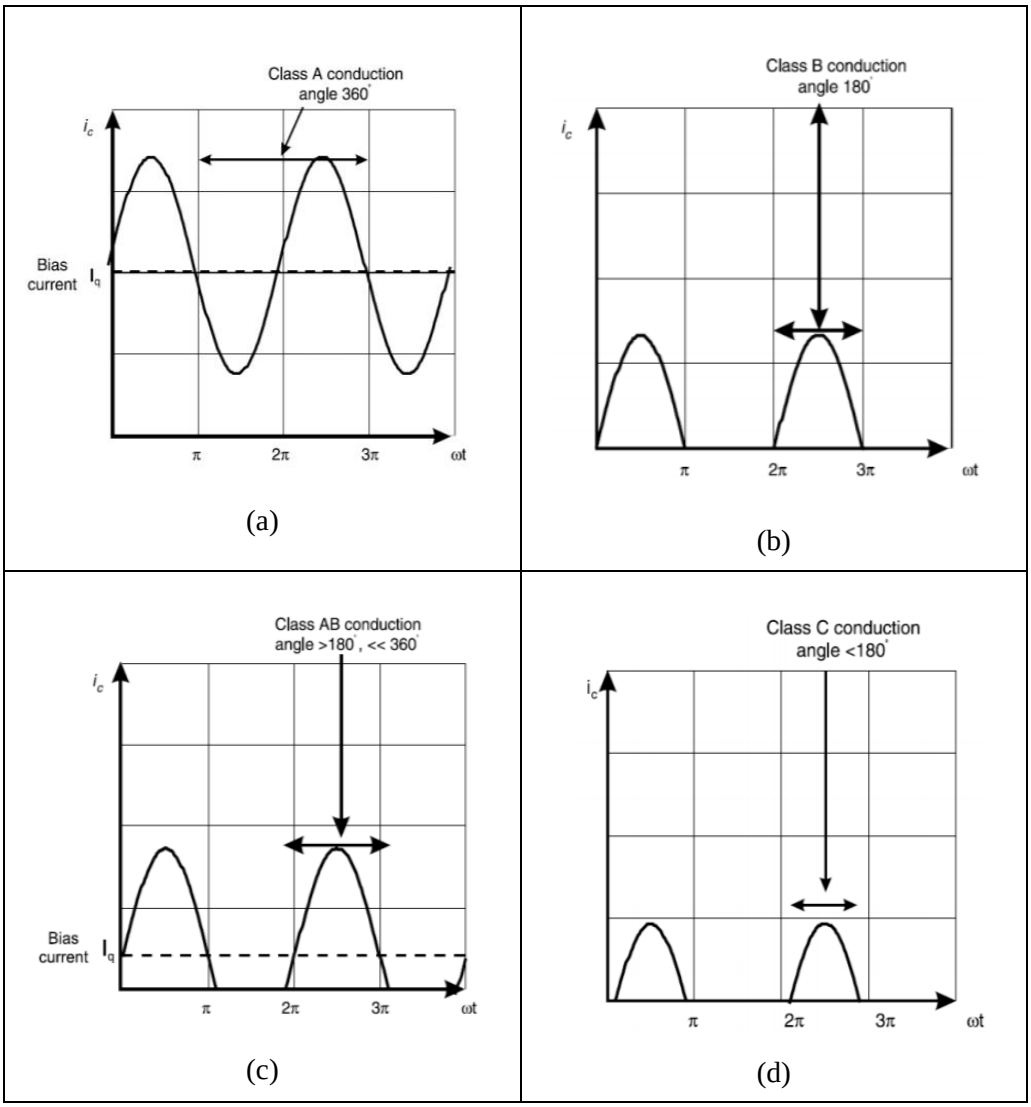

Figure 5: conduction angles for different power amplifier classes [10]: (a) class A, (b) class B, (c) class AB (d) class C

Class AB, Figure 5 (c), is an intermediate class between A and B, with a drain current conduction angle between 180° and 360°. Higher than *50%* efficiency is recorded for these amplifiers, but they

have lower distortion. In class C, Figure 5 (d), the drain conduction angle is less than 180°, which means higher efficiency than class A and B, but they have nonlinear behavior [5].

For different amplifiers' classes, the efficiency can be calculated as

$$\eta = \frac{\theta - \sin\theta}{4\left(\sin\left(\frac{\theta}{2}\right) - \left(\frac{\theta}{2}\right)\cos\left(\frac{\theta}{2}\right)\right)} \tag{3}$$

where θ is the conduction angle of the drain current.

2.4 Non-linearity of PA

In this part, the non-linearity of PA is explained. Normally, PA is intended to amplify the RF input signal, v_i, to produce the amplified RF output signal, v_o. Hence, the relationship can be characterised as

$$v_o = G\, v_i \tag{4}$$

where G is the ideal gain. The above relationship is linear. However, perfectly ideal PA does not exist. Since the PA start to act nonlinearly after the 1 dB compression point, and hence, it produces spectral regrowth, it is explained in next subsections. For showing this, a non-linear device block is assumed to model the PA with an input v_i and an output v_o.

Then, the output response can be represented by a Taylor series [12] as follow:

$$v_o = a_0 + a_1 v_i + a_2 v_i^2 + a_3 v_i^3 + \cdots. \tag{5}$$

where the Taylor expansion coefficients are defined as [12]

$$a_0 = v_o(0) \qquad \textit{(DC output)} \tag{6}$$

$$a_1 = \left.\frac{d\, v_o}{d\, v_i}\right|_{v_i=0} \qquad \textit{(linear output)} \tag{7}$$

$$a_2 = \left.\frac{\boldsymbol{d^2}\, v_o}{\boldsymbol{d}\, v_i^2}\right|_{\boldsymbol{v_i=0}} \qquad \textit{(squared output)} \tag{8}$$

2.4.1 Gain Compression

To study the compression point, the input to a power amplifier is assumed to be a single frequency sinusoid signal, as shown below

$$v_i = V_o \cos w_0 t \tag{9}$$

where V_o and w_0 are amplitude and angular frequency of the input signal, respectively. By substituting (9) in (5), the output can be expressed as

$$v_o = a_0 + a_1 V_o \cos w_0 t + a_2 V_o^2 \cos^2 w_0 t + + a_3 V_o^3 \cos^3 w_0 t + \cdots. \tag{10}$$

By rearranging (10), v_o is defined as

$$v_o = \left(a_0 + \frac{1}{2}a_2V_o^2\right) + \left(a_1V_o + \frac{3}{4}a_3V_o^3\right)cos\ w_0t + \frac{1}{2}a_2V_o^2cos\ 2w_0t + \frac{1}{4}a_3V_o^3cos\ 3w_0t + \cdots \quad (11)$$

The voltage gain (i.e., the ratio between the output and input) at the fundamental frequency, (w_0), can be obtained from

$$G_v = \frac{v_o^{(w_0)}}{v_i^{(w_0)}} = \frac{a_1V_o + \frac{3}{4}a_3V_o^3}{V_o} = a_1 + \frac{3}{4}a_3V_o^2 \quad (12)$$

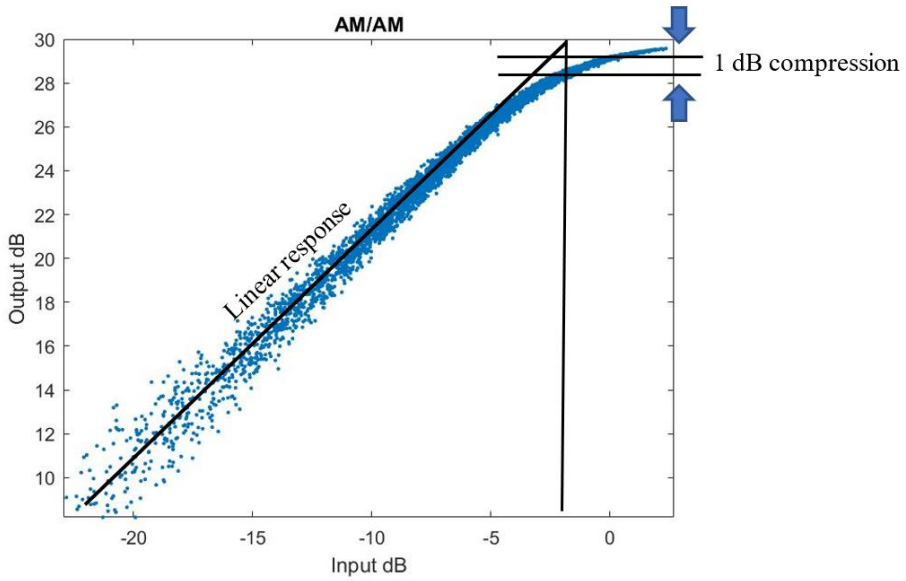

Figure 6: Output response of a typical power amplifier

It is observable that the gain, G_v, equals a linear coefficient, a_1, in addition to a term proportional to the input voltage. In most practical amplifiers, a_3, has the opposite sign of a_1. Hence the output of an amplifier starts to be reduced from its expected output ($G_v \times$ input) for a large input value, V_o. This effect is known as gain *compression* or *saturation* [12]. Figure 6, shows AM/AM plot that clarifies how the amplifier gain is going to saturate over a limited linear region of operation. These measurements are taken from one transmitter branch based on only input and output signals of PA. The *1 dB compression point* is where the output power level is decreased by 1 dB from its ideal linear characteristic.

2.4.2 Intermodulation (out of-band) distortion

The nonlinear behavior of PA introduces spectral regrowth in frequency domain to the RF output signal compared to input signal. To study that, the input signal, v_i, in (9), is replaced with two-tone signal

$$v_i = V_o(cos\ w_1t + cos\ w_2t) \quad (13)$$

After substituting in (4), the output spectrum response consists of harmonics of the form [12]

$$mw_1 + nw_2 \tag{14}$$

where m, n = 0, ±1, ±2, ±3, ... These combinations are called *intermodulation products* of the *order* equal to $|m| + |n|$. These products are not desired in power amplifiers output, because they appear as a spectrum regrowth and interfere with adjacent signals spectrum. Even order products are located far away from the fundamental zone and they can be easily filtered using either band pass or band stop filters. Some of the odd order products are located close to the original input signal and they are hard to be filtered out [13], e.g., third order. Figure 7 illustrates the second and the highlighted third order intermodulation products [12].

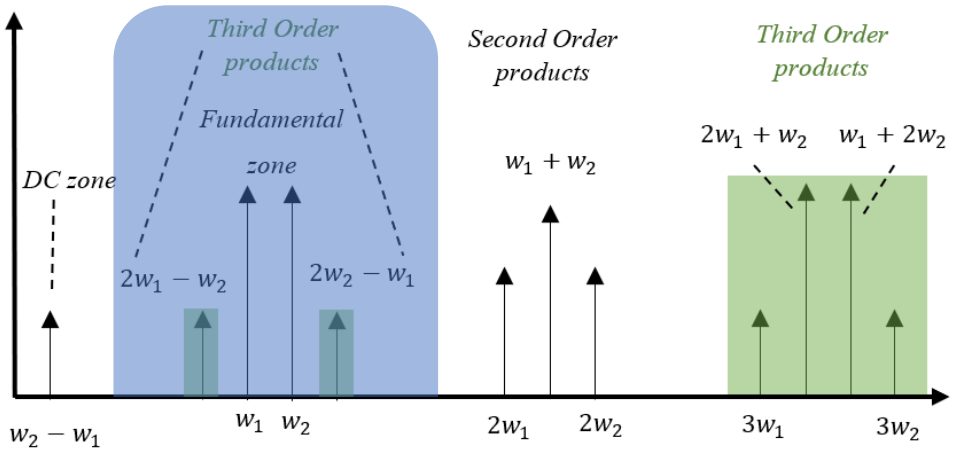

Figure 7: Output spectrum of the second- and third-order two-tone intermodulation products [12]

When introducing a wide band communication signal to a power amplifier, the output signal with a noticeable frequency regrowth will present. This behavior is known as the out-of-band distortion, as illustrated in Figure 8.

To measure this type of distortion the *Adjacent Leakage Ratio* (*ACLR*) can be used (15). ACLR is a figure of merit that indicates the ratio between the power intermodulation signal and the main signal. In other words, it can be defined as the ratio between the power within adjacent channel to the power of the transmitted signal within desired or main channel [14]. Both the desired and the adjacent channel are assumed to have the same bandwidth. ACLR is a term that used in the standardization of the 3GPP.

$$ACLR = \frac{\int_{BW_{adj}} |Y(f)|^2 df}{\int_{BW_{main}} |Y(f)|^2 df} \tag{15}$$

where $Y(f)$ is the transmitted signal in the frequency domain, BW_{adj} is the signal bandwidth of the adjacent channel and BW_{main} is the signal bandwidth of the main channel, and $BW_{adj} = BW_{main}$.

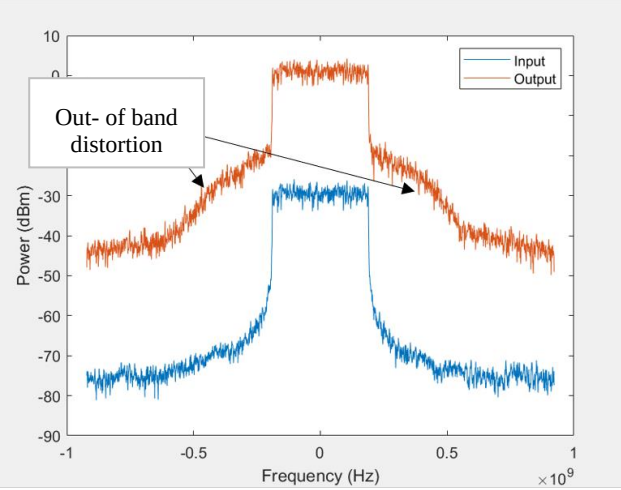

Figure 8: Frequency regrowth as a result of power amplifier non-linearity

2.4.3 In-band Distortion

The *Normalized Mean Square Error (NMSE)* is a figure of merit that indicates the difference between the actual measurement and the desired received signal as illustrated in (16). The NMSE is a measure of DPD performance. It can be determined as the deviation of the desired output, Y_{desired}, from the actual signal after using the linearization technique, Y_{actual}. Y_{desired} is scaled version of the input signal. In fact, NMSE is a measurement of both in- and out of band distortion, however, since the in-band distortion power is dominating the error, NMSE is dominated by in-band distortion and it can be mainly used as a measure of in-band distortion [29], as shown in Figure 9.

$$NMSE_{(Y_{desired}-Y_{actual})} = \frac{\|Y_{desired} - Y_{actual}\|_2}{\|Y_{desired}\|_2} \tag{16}$$

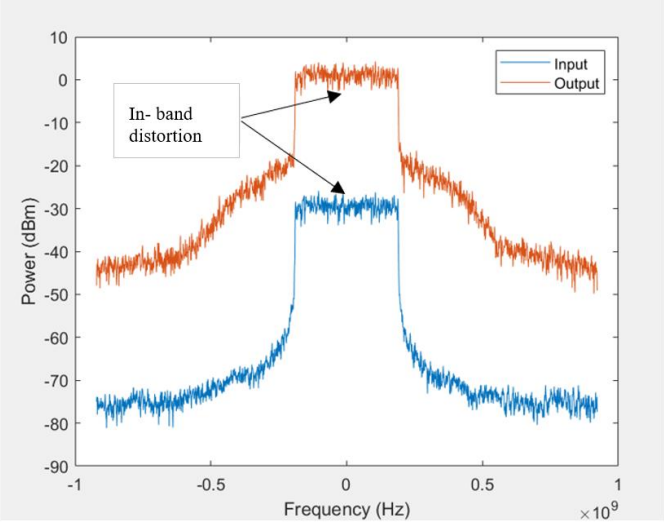

Figure 9: In-band distortion as a result of power amplifier non-linearity

2.4.4 Memory Effects on PA

Power amplifiers are non-linear devices with memory effects. Which means that the current output does not depend solely on the current input, but it also depends on the previous inputs. This memory effect comes from the physics of transistors that contains a number of energy-storing elements, e.g., capacitors. An example of such schematic can be illustrated in Figure 10. It is a small-signal model for a microwave FET, which included

transconductance g_m, output resistance r_0 and parasitic capacitance (c_{gs}, C_{ds}, and C_{gd}). Therefore, this memory effect causes delays in transient signal before reaching its steady state.

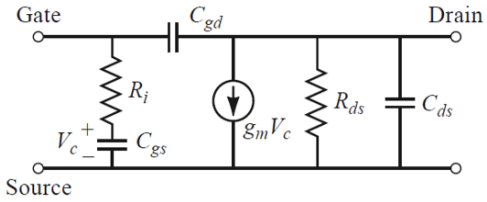

Figure 10: Small-signal equivalent circuit for a microwave FET in the common-source configuration [12]

The memory effect of a capacitor can be seen from the voltage equation (17) [15].

$$v_C(t) = \frac{1}{C}.\int_{-\infty}^{t} i(t').dt' \tag{17}$$

where $v_C(t)$ is the capacitor voltage at time t, C is the total capacitance for the small-signal equivalent circuit, $i(t')$ is the capacitance's current at previous time instance, t', which varies from $-\infty$ till the current time t.

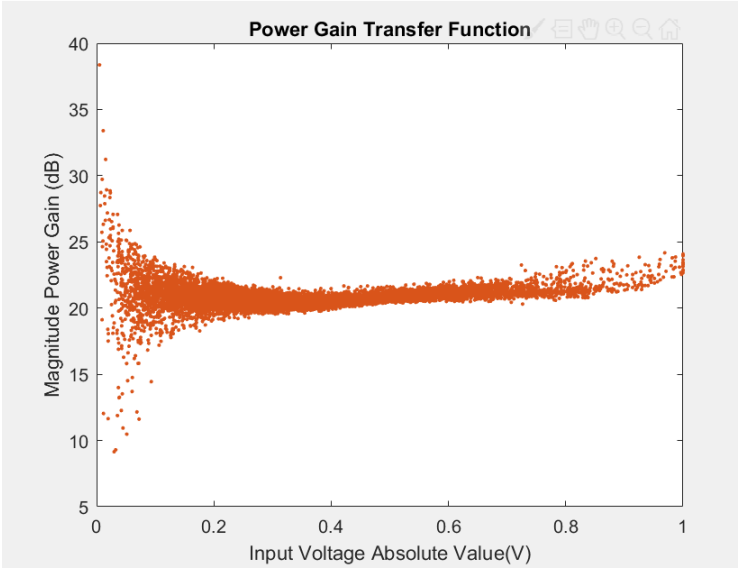

Figure 11: Memory effect on PA appears as a scattering in its characteristic curve

Thus, the non-linearity of PAs becomes worse in the presence of a strong memory effect. Figure 11 shows a magnitude characteristic of a commercial PA. The red curve dispersion (scattering) around the curve is due to PA's memory effect.

3

Power Amplifier Behavioural Modelling

An accurate PA behavior model is important to perform high-performance DPD. As explained earlier, both mismatch and crosstalk have an impact on PA behavior. Hence, it is important to consider the 2nd indirect input, which corresponds to mismatch and crosstalk. In this chapter, a behavioural model for both single-Input and dual-Input PA is presented. Furthermore, the extraction of model's parameters is explained.

3.1 Power Amplifier Modeling

Different models have been proposed over past years to model PA behavior. The most common one is Volterra series. It considers both nonlinearity and the memory effects of PA [16].

Band-limited signals are used in this thesis, which has a bandwidth between an order of kHz to tens of MHz while, the carrier frequency is in the sub-6 GHz bands (mid-band). The signals are commonly presented in a complex-valued baseband form and the signals samples are assumed to be i.i.d. Hence, the discrete-time complex baseband Volterra model with order P for SISO PA model is written as [16]

$$b(n) = \sum_{p=1}^{P} \sum_{m_1=0}^{M_1} \cdots \sum_{m_p=m_{p-1}}^{M_p} \sum_{m_{p+1}=0}^{M_{2p+1}} \cdots \sum_{m_{2p-1}=m_{2p-2}}^{M_{2p-1}} \theta_{pm_1m_2\cdots m_{2p-1}} \times a(n-m_1)\cdots a(n-m_p)\, a(n-m_{p+1})^* \cdots a(n-m_{2p-1})^* \tag{18}$$

where, $a(n)$ and $b(n)$ are complex baseband input and output signals of the PA, respectively, $(.)^*$ is complex conjugate, M_i is the memory depth for i^{th} tap and θ_{2p-1} is the p^{th} order complex Volterra kernel. Due to kernel symmetry, redundant kernels are removed, i.e., $\theta_{pm_1m_2\,m_3} = \theta_{pm_1m_3m_2}$. Even orders are ignored in this equation since it can be simply filtered out using either band rejection or bandpass filters, as it was explained earlier in section 2.4.2. In this model, the number of conjugate and non-conjugated terms differ by one for the fundamental frequency components. Modeling using Volterra series is not applicable and complex. This is because the numbers of coefficients are high to fully implement the Volterra series to model the PA. Therefore, it can be simplified to Memory Polynomial (MP) model [16]. In this model, the cross-terms between the input signal and its terms with different delays are pruned to be

$$b(n) = \sum_{\substack{p=1 \\ p\ is\ odd}}^{P} \sum_{m=0}^{M} \theta_{pm} a(n-m)|a(n-m)|^{p-1} \tag{19}$$

In matrix form, the above formula is rewritten as

$$\boldsymbol{b} = \boldsymbol{H}(\boldsymbol{a})\boldsymbol{\theta} \tag{20}$$

where $\boldsymbol{a}$ and $\boldsymbol{b}$ are vectors containing N time samples, e.g., $\boldsymbol{a} = [a(0), a(1), \cdots, a(N-1)]$. And $\boldsymbol{H}$ is matrix basis function or regression matrix having size of $(N \times \frac{(P+1)(M+1)}{2})$, and $\boldsymbol{\theta}$ is vector of complex coefficients $(N \times 1)$.

The above SISO MP model for PA does not consider the 2nd input that corresponds to crosstalk and mismatch contributions. These two effects are briefly explained in sections 3.2 and 3.3, respectively. This will be followed by the dual-input PA modelling for MIMO case, i.e., MIMO PA model.

3.2 Mutual Coupling (Cross-talk)

In MIMO communication systems, multiple branches in the transmitter chain are susceptible to different levels of coupling between each other due to cross-talk effects. The coupling concept can be simply represented in Figure 12. In coupling or cross-talk, a part of the radiated wave through the antenna is leaked to another branch or multiple branches in case of MIMO systems.

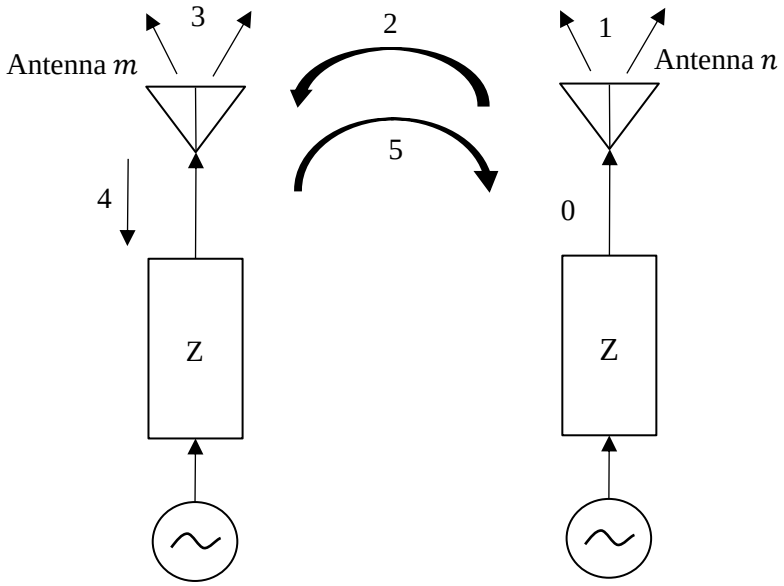

Figure 12: Mutual coupling between antennas

Assuming two antennas in a transmitter chain, where antenna 'n' is excited by a source (active), while antenna 'm' is not transmitting (passive). The generated signal towards antenna element 'n' is indicated as (0) in the graph and then it radiates to free space, which is labeled as (1). A portion of this energy is transferred to antenna 'm', label (2). A signal is then induced in antenna 'm' which causes this antenna to radiate amount of energy into free space, which is labeled as (3). Then, a part of this energy will be dissipated on the passive load of antenna 'm'. Subsequently, antenna 'n' will receive a portion of the energy radiated by antenna 'm'. This process will continue infinitely. When both antennas 'm' and 'n' are excited, the total radiated field is the summation of the radiated and re-scattered fields from both antenna elements [17]. In MIMO systems with multiple branches, the amount of coupling is proportional to the distance between branches. The leakage power to the nearby branch is much higher than the leakage power to the distant branch. As a result, this cross-talk coupling has a great impact on the performance of PA [18], it mixes with PA output. As a result, a spectrum regrowth is noticed, and distortion is introduced to the modulated RF signal [18].

3.3 Impedance Mismatch

The amplified RF signal after PA, as illustrated earlier, propagates through the wave guide or the transmission line before reaching the antenna element. When both impendences of PA and antenna are different, a portion of amplified signal get reflected towards the PA, i.e., mismatch. This phenomenon leads to power losses and attenuation in the signal [12]. Figure 13, illustrates the mismatch between PA impedance (Z_{amp}) and antenna impedance (Z_{ant}).

The reflection coefficient can be calculated as [12];

$$\Gamma_l = \frac{Z_{ant} - Z_{amp}}{Z_{ant} + Z_{amp}} \tag{21}$$

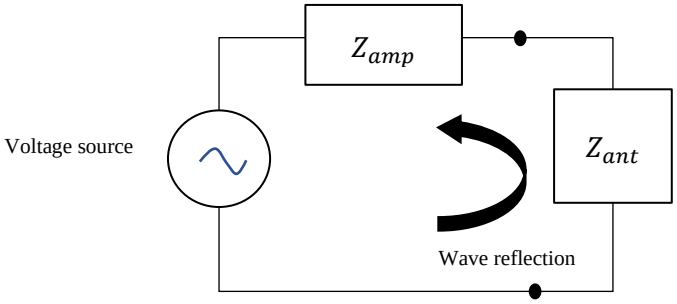

Figure 13: Reflection in incidence wave due to impedances mismatch [12]

3.4 Crosstalk and Mismatch in Antenna Array

In multi antenna systems, as shown in Figure 14, the crosstalk and mismatch signal at k^{th} branch, $\boldsymbol{a_{2k}}$, can be represented as a function of the PA outputs, $\boldsymbol{b_{2k}}$, where both $\boldsymbol{a_{2k}}$ and $\boldsymbol{b_{2k}}$ are vectors contains all *N* time samples. The antennas are wideband compared to the signal bandwidth. Hence, the single-frequency S-parameters, $\boldsymbol{\lambda_k}$, [16] is used to define the relation between $\boldsymbol{a_{2k}}$ and the PA output signals of all transmit branches, $\mathbf{b_2}$. Hence, $\boldsymbol{a_{2k}}$ is described as

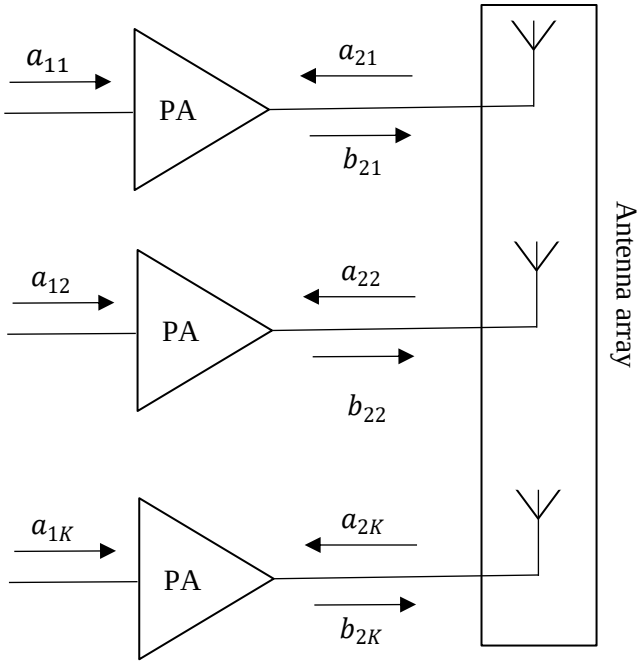

Figure 14 Multi-antenna transmitter system model [16]

$$\boldsymbol{a_{2k}} = \boldsymbol{b_2}^{\boldsymbol{T}}.\boldsymbol{\lambda_k} \tag{22}$$

where $\boldsymbol{b_2} = [\boldsymbol{b_{21}}, \dots, \boldsymbol{b_{2k}}]^T$ and $\boldsymbol{\lambda_k} = [\boldsymbol{\lambda_{k1}}, \dots, \boldsymbol{\lambda_{kK}}]^T$. The S-parameter matrix, $\boldsymbol{\lambda_k}$, is measured at the center frequency, which is corresponds to a matrix $[\boldsymbol{\lambda_1}, \dots, \boldsymbol{\lambda_K}]$. And the $\boldsymbol{b_2}$ is a matrix with dimensions of $K \times N$. To prevent power amplifiers from this mutual coupling or crosstalk effect, isolators is inserted in each branch between PA and antenna. However, these isolators are bulky and very costly to be integrated in the transmitter, which it is explained in Appendix 9.2 in detail.

3.5 Dual-Input PA Modeling

The SISO MP model does not consider the cross talk and mismatch effects, and hence it is not valid to be used anymore, where it is challenging to have high isolation level to ban these effects. Hence, it is crucial to model the PA with respect to cross talk and mismatch effects. In [16], dual-input Volterra series model is used to model PA behavior. This model considers both direct input, $a_{1k}(n)$, and indirect input, $a_{2k}(n)$, which is corresponding to the cross talk and mismatch effects. The output signal, $b_{2k}(n)$, based on this model is written as [16]

$$
\begin{aligned}
&\mathrm{b_{2k}(n)} = \sum_{\mathrm{m=0}}^{\mathrm{M}} \theta_{\mathrm{k000m_1}}\, \mathrm{a_{1k}(n-m_1)} + \sum_{\mathrm{m=0}}^{\mathrm{M}} \theta_{\mathrm{k010m_1}}\, \mathrm{a_{2k}(n-m_1)} && \text{A}\\
&+ \sum_{\mathrm{m_1}}^{\mathrm{M}}\sum_{\mathrm{m_2}}^{\mathrm{M}}\sum_{\mathrm{m_3}}^{\mathrm{M}} \theta_{\mathrm{k100m_1m_2m_3}}\, \mathrm{a_{1k}(n-m_1)a_{1k}(n-m_2)a_{1k}^{*}(n-m_3)} && \text{B}\\
&+ \sum_{\mathrm{m_1}}^{\mathrm{M}}\sum_{\mathrm{m_2}}^{\mathrm{M}}\sum_{\mathrm{m_3}}^{\mathrm{M}} \theta_{\mathrm{k101m_1m_2m_3}}\, \mathrm{a_{1k}(n-m_1)a_{1k}(n-m_2)a_{2k}^{*}(n-m_3)} && \text{C}\\
&\sum_{\mathrm{m_1}}^{\mathrm{M}}\sum_{\mathrm{m_2}}^{\mathrm{M}}\sum_{\mathrm{m_3}}^{\mathrm{M}} \theta_{\mathrm{k110m_1m_2m_3}}\, \mathrm{a_{1k}(n-m_1)a_{2k}(n-m_2)a_{1k}^{*}(n-m_3)} && \text{D}\\
&+ \sum_{\mathrm{m_1}}^{\mathrm{M}}\sum_{\mathrm{m_2}}^{\mathrm{M}}\sum_{\mathrm{m_3}}^{\mathrm{M}} \theta_{\mathrm{k111m_1m_2m_3}}\, \mathrm{a_{1k}(n-m_1)a_{2k}(n-m_2)a_{2k}^{*}(n-m_3)} && \text{E}\\
&+ \sum_{\mathrm{m_1}}^{\mathrm{M}}\sum_{\mathrm{m_2}}^{\mathrm{M}}\sum_{\mathrm{m_3}}^{\mathrm{M}} \theta_{\mathrm{k120m_1m_2m_3}}\, \mathrm{a_{2k}(n-m_1)a_{2k}(n-m_2)a_{1k}^{*}(n-m_3)} && \text{F}\\
&+ \sum_{\mathrm{m_1}}^{\mathrm{M}}\sum_{\mathrm{m_2}}^{\mathrm{M}}\sum_{\mathrm{m_3}}^{\mathrm{M}} \theta_{\mathrm{k121m_1m_2m_3}}\, \mathrm{a_{2k}(n-m_1)a_{2k}(n-m_2)a_{2k}^{*}(n-m_3)} && \text{G}\\
&+ \cdots
\end{aligned}
\tag{23}
$$

The linear kernels in (A) is given for each input signal. The self-kernels in (B) and (G) have same symmetry property as SISO Volterra. The cross terms in (C) and (F) have symmetry property, i.e., $\theta_{k101m_1m_2m_3} = \theta_{k101m_2m_1m_3}$, but not for permutations of m_1, m_2, m_3. The kernels in (D) and (I) corresponds to frequency domain Volterra kernel being excited in $\theta_{k110\, w_{c1}\, w_{c2}\, -w_{c1}}$ and $\theta_{k111\, w_{c1}\, w_{c2}\, -w_{c1}}$. The above formula can be re-written as follow,

$$
\begin{aligned}
b_{2k}(n) &= \sum_{q_1}^{1}\sum_{m_1=0}^{M} \theta_{k0q_10m_1} \left(a_{1k}(n-m_1)\right)^{1-q_1} \times \left(a_{2k}(n-m_1)\right)^{q_1}\\
&+ \sum_{p=1}^{\left(\frac{P-1}{2}\right)} \sum_{q_1=0}^{p+1} \sum_{q_2}^{p} \sum_{m_1}^{M} \cdots \sum_{m_{p+1-q_1}=m_{p-q_1}}^{M} \sum_{m_{p+1-q_1}=0}^{M} \cdots \sum_{m_{p+1}=m_p}^{M} \sum_{m_{p+2}=0}^{M} \cdots\\
&\sum_{m_{2p+1-q_2}=m_{2p-q_2}}^{M} \sum_{m_{2p+2-q_2}=0}^{M} \cdots \sum_{m_{2p+1}=m_{2p}}^{M} \theta_{kpq_1q_1m_1m_2\cdots m_{2p+1}}\\
&\times \prod_{i=1}^{p+1-q_1} a_{1k}(n-m_i) \prod_{l=p+2-q_1}^{p+1} a_{2k}(n-m_l) \prod_{s=p+2}^{2p+1-q_2} a_{1k}^{*}(n-m_s) \prod_{r=2p+2-q_2}^{2p+1} a_{2k}^{*}(n-m_r)
\end{aligned}
\tag{24}
$$

where the terms q_1 and q_2 are used for better definition of cross terms. M and P are memory depth and nonlinear order respectively. Like SISO case, due to high complexity of model, the full Volterra series is inapplicable. Hence, Volterra model is reduced to Memory Polynomial (MP) model. In this structure, cross terms between the direct signal and it is terms with different delays are not considered in MP. Hence, MP version of above formula can be re-written as [16]

$$\begin{aligned} b_{2k}(n) = & \sum_{m_1}^{M_1} \sum_{p=0}^{\frac{(P_1-1)}{2}} \alpha_{m_1}^{(2p+1)} a_{1k}(n-m_1)|a_{1i}(n-m_1)|^{2p} + \sum_{m_2=0}^{M_2} \beta_{0\,m_2}^{(1)} a_{2k}(n-m_2) \\ & + \sum_{m_3=0}^{M_3} \sum_{m_3=0}^{M_4} \sum_{p=1}^{\frac{(P_2-1)}{2}} \beta_{m_4 m_3}^{(2p+1)} a_{2k}(n-m_3)|a_{1k}(n-m_4)|^{2p} \\ & + \sum_{m_3=0}^{M_5} \sum_{m_3=0}^{M_6} \sum_{p=1}^{\frac{(P_3-1)}{2}} \gamma_{m_6 m_5}^{(2p+1)} a_{2k}^*(n-m_3)\big(a_{1k}(n-m_1)\big)^{p+1}\big(a_{1k}^*(n-m_1)\big)^{p-1} \\ & + \sum_{m_7=0}^{M_7} \sum_{m_8=0}^{M_8} \sum_{p=1}^{\frac{(P_4-1)}{2}} \sum_{v=0}^{p} \sum_{\substack{u=0 \\ u>1-v}}^{p+1} \delta_{u\,v\,m_8 m_7}^{(2p+1)} \big(a_{1k}(n-m_7)\big)^{p+1-u}\big(a_{1k}^*(n-m_1)\big)^{p-v} \times \\ & \big(a_{2k}(n-m_8)\big)^{u}\big(a_{1k}^*(n-m_8)\big)^{v} \end{aligned} \tag{25}$$

where $P_1, P_2, P_3,$ and P_4 are nonlinear orders, and $M_1, M_2, M_3, M_4, M_5, M_6, M_7,$ and M_8 are memory depths. And $\boldsymbol{\alpha}$, $\boldsymbol{\beta}$, $\boldsymbol{\gamma}$, and $\boldsymbol{\delta}$ are vectors corresponds to complex coefficients. The above formula can be written in matrix format as

$$\boldsymbol{b_2} = \boldsymbol{H}(\boldsymbol{a_1}, \boldsymbol{a_2})\, \boldsymbol{\theta} \tag{26}$$

where $\boldsymbol{b_2}$, $\boldsymbol{a_1}$ and $\boldsymbol{a_2}$ are vectors including all N time-samples. For instance, $\boldsymbol{b_2} = [b_2(0), \cdots, b_2(N-1)]^T$, $\boldsymbol{H}(\boldsymbol{a_1}, \boldsymbol{a_2})$ is the basis function and $\boldsymbol{\theta}$ is the complex coefficients vector that corresponds to $\boldsymbol{\alpha}$, $\boldsymbol{\beta}$, $\boldsymbol{\gamma}$, and $\boldsymbol{\delta}$. i.e., $\boldsymbol{\theta} = \left[\boldsymbol{\alpha}^T\, \boldsymbol{\beta}^T\, \boldsymbol{\gamma}^T\, \boldsymbol{\delta}^T\right]^T$.

3.6 Model Extraction

To model the PA output for a given input, coefficients are needed to be extracted. The regression matrix, $H(.)$, depending on the direct input for SISO MP model (20) or on the dual inputs for dual input MP model (26), hence bellow equation can be used.

$$\boldsymbol{b} = \boldsymbol{H}\, \boldsymbol{\theta} \tag{27}$$

where $\boldsymbol{\theta}$ is the model coefficients and $\boldsymbol{b}$ is the output, as shown below,

$$\boldsymbol{b} = [\boldsymbol{b}(\boldsymbol{0}), \ldots, \boldsymbol{b}(\boldsymbol{N-1})]^{\boldsymbol{T}} \tag{28}$$

The model coefficients, $\boldsymbol{\theta}$, is estimated using the least square method [16], as

$$\boldsymbol{\theta} = \boldsymbol{H}^{+}\boldsymbol{b} \tag{29}$$

$H^{+}$is Moore-Penrose pseudoinverse, which is calculated as

$$\boldsymbol{H}^{+} = (\boldsymbol{H}^{\boldsymbol{H}}\boldsymbol{H})^{-1}\boldsymbol{H}^{\boldsymbol{H}} \tag{30}$$

where $(.)^{H}$ is the conjugate transpose (i.e., Hermitian) and $(.)^{-1}$ is the matrix inverse.

3.7 Model accuracy

To test the accuracy of the model, the NMSE between the measured, $\boldsymbol{b_{measured}}$, and modeled output, $\boldsymbol{b_{modeled}}$, using the extracted model, is calculated as [14]

$$NMSE_{(b_{measured}-b_{modelled})} = \frac{\|\boldsymbol{b_{measured}} - \boldsymbol{b_{modelled}}\|_2}{\|\boldsymbol{b_{measured}}\|_2} \tag{31}$$

The selection of memory depths and polynomial orders is determined by the targeted NMSE level, it will be explained further in chapter 5. As stated previously, the 2nd input is important to model the output. However, the 2nd input depends on the output, due to mismatch contributions. To address that, the authors in [18], the author presented prediction structure for the output by considering the direct input and the S-matrix only. In our case, the $\boldsymbol{a_{2k}}$ is given and there are no mismatch effects, it will be explained later.

4

PA Linearization

The nonlinear behavior of PA causes spectrum regrowth to the amplified RF signal (out-band distortion). Furthermore, it causes in-band distortion which increases BER and EVM. With these distortions, 3GPP requirements will be mostly violated for the sub-6 GHz radios. Hence, it is crucial to linearize the output of the PA to reduce these two kinds of distortions.

There are many existing solutions to achieve the PA linearization. Among various linearization techniques, the most popular solution is the Digital Predistortion (DPD). In this chapter, different linearization techniques of PA are presented. Then, the DPD methods that based on closed and open loop are discussed.

4.1 Linearization Techniques

The linearization of PAs becomes a necessity to guarantee that the transmitted signal does not interfere harmfully with the adjacent channels that belong to other users or systems. To address the nonlinearity issue, the power amplifier can be backed off to operate within its linear region. However, backing off the transmitted power reduces the efficiency of PAs. As a result, linearization is an efficient method to improve the PA efficiency without compromising the 3GPP regulations.

There are numerous linearization techniques that differ in complexity, advantages, and limitations. Choosing the linearization technique depends on the application of the communication system itself. For instance, a high complex linearization method is used in base stations, while a low complex technique is suitable for handsets. Those techniques can be categorized into three groups: feedback, feedforward and digital pre-distortion (DPD).

4.1.1 Feedback Method

This technique is the simplest way to linearize PAs [19], which is defined as analogue post distortion. The principal idea of this method is to force the output to follow the input of the PA. Mainly, two types of feedback can be used: RF and modulation feedback, which is divided into two: polar and Cartesian feedback. In RF feedback, the RF signals are compared without modulation, whereas in modulation feedback the input and output modulation components (I and Q) are compared. Feedback method can be exploited at RF, IF or baseband frequencies. Figure 15 shows the feedback linearization method. The controller takes a portion of the output signal from the PA. This portion is the fed back and subtracted from the PA input signal to optimize the output to be a linear version of the input signal.

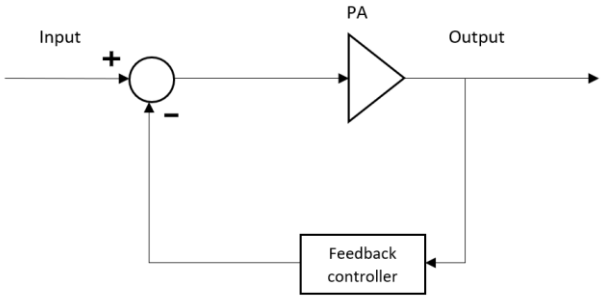

Figure 15: Feedback linearization method contains a feedback controller and a summing circuit to optimize the output

4.1.2 Feedforward Method

The idea behind this method, is to extract RF PA output distortion, amplify it and add it to the PA output in the opposite phase to cancel the distortion [19]. This method has a low power efficiency due to a high-power requirement of the error amplifier (class A) which needs to be a linear, and there is

power loss due to the couplers. Furthermore, it has an advantage of reducing the distortion over a wide bandwidth.

4.2 DPD Linearization Technique

The idea behind this technique is to pre-process an input signal before introducing it to the PA in such a way that it compensates the nonlinearities [13]. Figure 16 illustrates the basic idea behind this method, where the pre-distorter has an inverse input-output nonlinear characteristic (i.e., nonlinear behavior). Then, the output signal is a linearized and amplified version of the RF input signal [20]. By doing this the PA nonlinearity can be compensated, as shown in Figure 16.

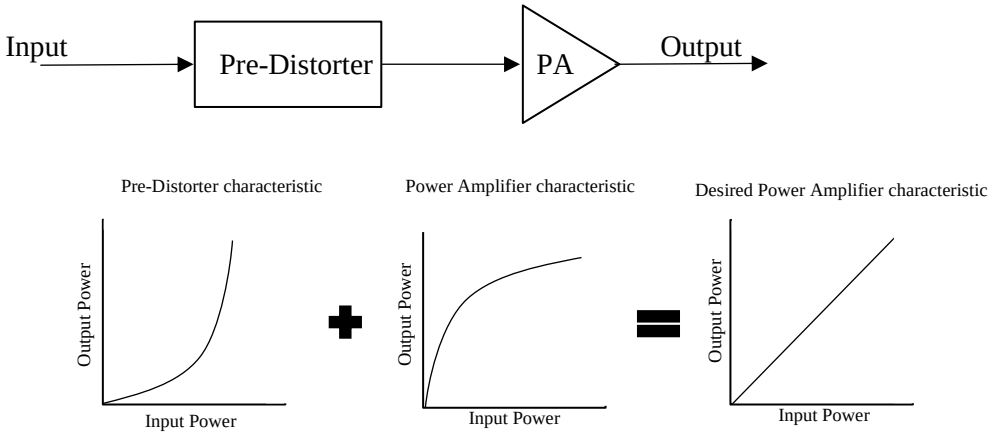

Figure 16: Predistortion method, where a pre-distorter with an inverse characteristic of PA is added to compensate for the PA non-linearity

Different methods are used to identify the parameters of the DPD, such as the Direct Learning Architecture (DLA), Indirect Learning Architecture (ILA), and the Iterative Learning Control (ILC).

4.2.1 Direct Learning Architecture (DLA)

In this method, the pre-distorter parameters can be estimated with respect to error level. Error is defined as the mean squared distance between the original input signal and the scaled output of the PA, as shown in Figure 17. The PA output is scaled by $(1/G)$, where G is average or max gain, it will be explained further in Chapter 5. Various DLA algorithms can be used, and they provide unbiased parameter estimation but most of them are complex and have a slow convergence [20].

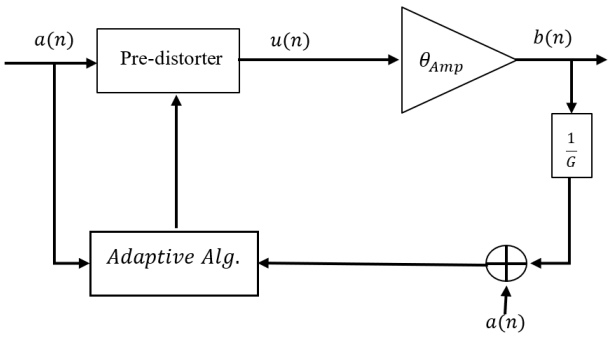

Figure 17: Block diagram illustrates the Direct Learning Architecture (DLA) algorithm

4.2.2 Iterative Learning Control (ILC)

ILC is a control theory technique [29] that is used to enhance the tracking of a system that operates iteratively over a fixed interval of time. Therefore, ILC is a technique that can be used to invert the dynamics of linear and nonlinear dynamical systems.

Figure 18 (a), illustrates the basic idea of this technique.

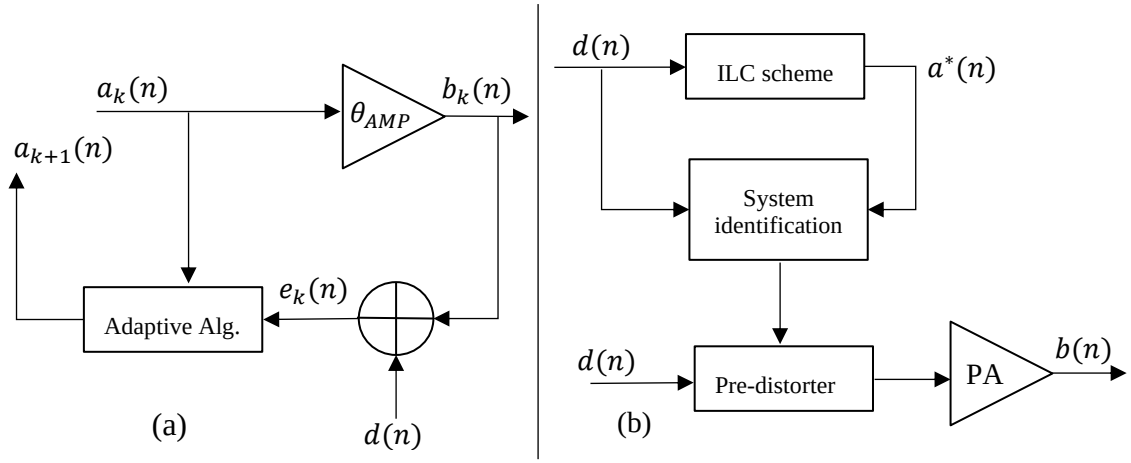

Figure 18: Iterative Learning Control (ILC) implementation algorithm: (a) ILC scheme (b) ILC-DPD scheme

The output from PA, $b(n)$, is desired to be as close as possible to the desired output $d(n)$ i.e., linearized version of $a(n)$ that is scaled with G. Therefore, the idea is to find the optimal input $a(n)$ that gives an output close to the desired one. This technique is executed iteratively until finding the optimal input [20], as shown for the k^{th} iteration,

$$a_{k+1} = a_k + \Delta e_k \tag{32}$$

where Δ is the learning matrix and e_k is the error between actual and desired output. ILC differs from other adaptive control methods as other techniques mostly modify either the controller or the parameters of this controller while ILC deals only with the input signal [29]. The main aim from the ILC scheme is to find the optimal input $a^*(n)$ that minimizes the error, $e_k(n)$, between the desired output, $d(n)$, and actual output of the PA, $b(n)$.

Above ILC scheme can identify the optimal input signal, $a^*(n)$, that linearizes the PA, but it does not provide a pre-distorter model. To address this issue, an ILC-DPD is proposed in [29]. The block diagram of ILC-DPD is shown in Figure 18 (b). ILC-DPD first uses an ILC scheme to find the optimal input signal, $a^*(n)$. Then, the parameters of the pre-distorter model are estimated using $d(n)$ as an input and $a^*(n)$ as an output.

4.2.3 Indirect Learning Architecture (ILA)

In this thesis, Indirect Learning Architecture (ILA), as shown in Figure 19, is used. It is based on the inverse of PA nonlinear modeling approach. ILA is a closed-loop iterative process that includes two main blocks: pre-distorter and post-distorter. The post-distorter block aims to estimate the model coefficients of PA that minimize the error, e.g., increase the ACLR. The coefficients of the post-distorter are determined using the output of the PA as the input, and the input to PA as the output. The extraction approach that was illustrated in section 3.6 is used here to find the coefficients of the post-distorter (i.e, Least Square (LS)). Then, these coefficients are used in pre-distorter block, i.e., DPD block. ILA simplifies the identification process of pre-distorter from a nonlinear optimization problem to an iterated linear optimization problem [22]. However, this method provides a limited performance when the PA nonlinearity is strong [23]. The estimated inverse of PA model is then placed just before the PA. ILA assumes that both forward (PA) and inverse (DPD) models have the same structure of bases functions, i.e., $H(.)$.

First step is modeling the PA by estimating model coefficients, θ_{Amp}, using the LS method. By implementing this process iteratively, a final version of the pre-distorter with coefficients θ_{DPD} is determined. The flowchart, as shown in Figure 20, describes the algorithm of DPD that uses the ILA method to linearize PA.

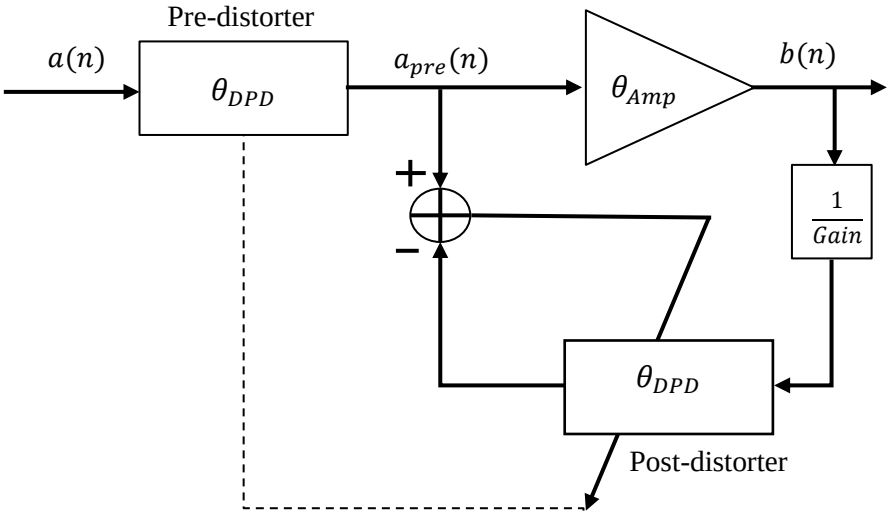

Figure 19: Iterative Learning Architecture algorithm

To implement DPD algorithm, firstly, the input signal, $a(n)$, is introduced to the PA without any pre-distortion. The output signal from PA is then captured.

To determine the PA inverse function, the output signal, $b(n)$, is normalized to be used as an input to the post-distorter, while the input, $a_{pre}(n)$, is used as an output. By utilizing least square solution, the coefficients of inverse model, $\boldsymbol{\theta_{DPD}}$, can be found, by using (33). In the next iteration, the input signal, $a(n)$, is then introduced to the pre-distorter block with exact coefficient of previous iteration. A pre-distorted signal, $a_{pre}(n)$, which represents the output from the pre-distorter block, is now treated as the input of the PA. This process is continued iteratively till it converges.

$$\boldsymbol{\theta_{DPD}} = \left(\boldsymbol{H}\left(\frac{\boldsymbol{b(n)}}{Gain}\right)\right)^{+} \boldsymbol{a_{pre}} \tag{33}$$

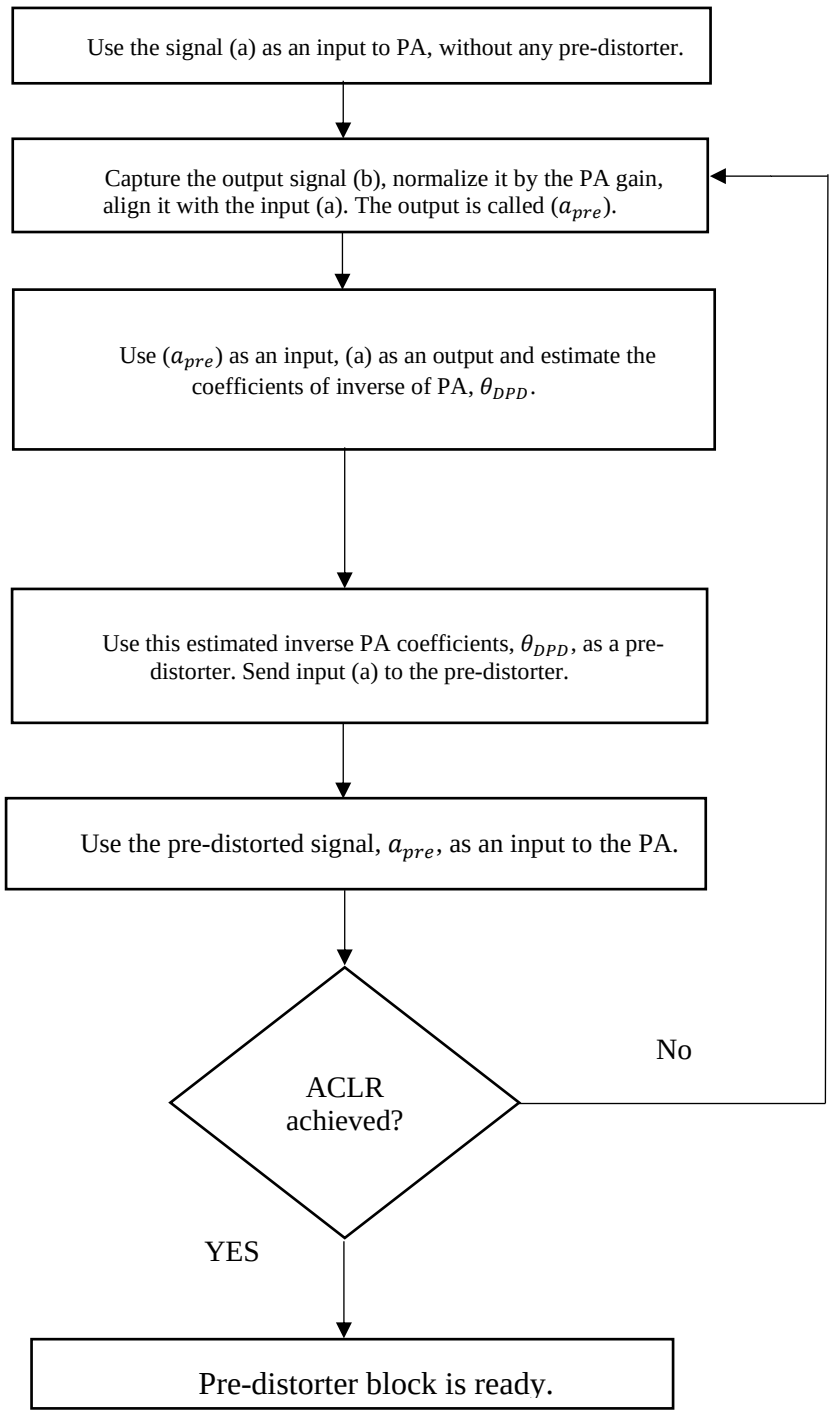

Figure 20: flow chart of DPD using ILA algorithm

As an example, PA measurements for single branch that suffer from nonlinear distortion are linearized using the above algorithm. The input signal is modulated with carrier frequency of 1.9 GHz and it has a bandwidth of 400 MHz. Due to PA nonlinearity, the output signal suffers from spectrum regrowth with respect to the input spectrum, as shown in Figure 21. The PA model coefficients, θ_{AMP}, are extracted using the SISO MP modelling approach, which is illustrated in section 3.6.

After applying ILA DPD algorithm, the Pre-distorter block coefficients, θ_{DPD}, is defined in an iterative process as explained above. Figure 21 illustrates the spectrum of input signal, measured output (i.e., output without DPD) signal and linearized output signal. It can be seen that the DPD compensates for the nonlinearity and reduces the spectral regrowth. The nonlinear behavior of a PA is commonly

shown via AM-AM (Amplitude/Amplitude) and AM-PM (Amplitude/Phase) conversions, [20]. They consist of the variations of the input amplitude into of the output amplitude and phase, respectively.

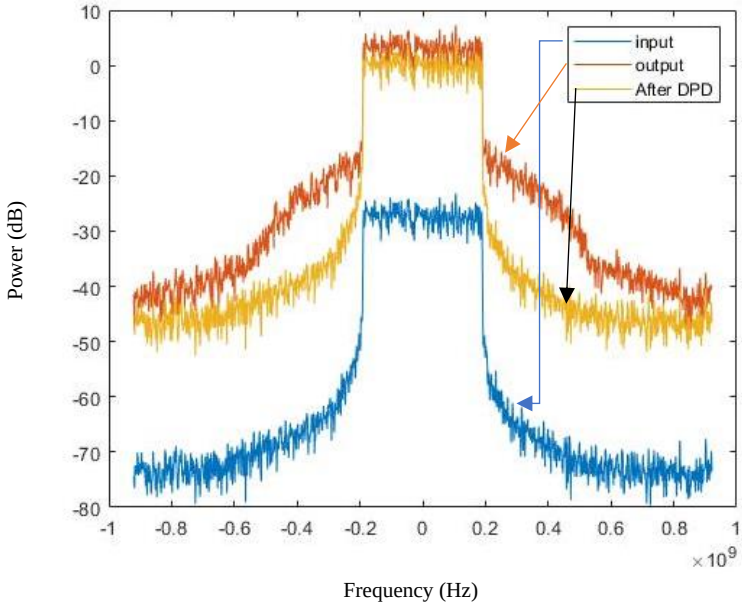

Figure 21: Input and output before and after DPD implementation

Figure 22 shows AM/AM and AM/PM curves for measured output, pre-distorted and linearized output signals. The pre-distorter has an inverse behavior of PA in terms of amplitude and phase, hence, the final output from the PA is linearized version of the input.

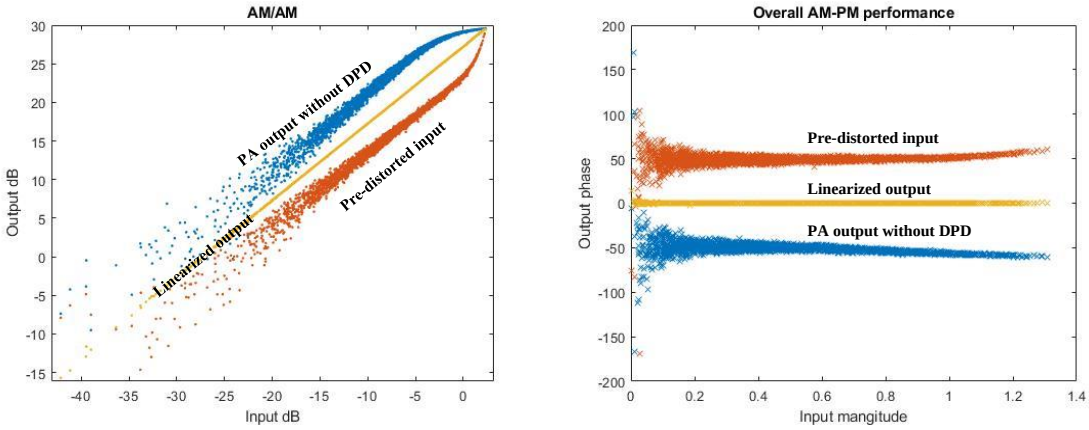

Figure 22: AM-AM and AM-PM curves illustrate pre-distorted, output and linearized signals

5

Implementation

To simulate all theoretical aspects which were described in previous chapters, the work in this project is divided into three main consecutive steps; PA modeling, DPD implementation and coupling influence investigation.

5.1 Source signal and Simulation Setup

The input signal is an OFDM signal at a carrier frequency of 3.6 GHz, with a sampling frequency of 1.8 GHz and a bandwidth of 400 MHz.

The response of the designed PA (22 nm FD-SOI CMOS) is simulated using Cadence simulator, as it can be seen in the simulation setup in Figure 23. In this setup, two radio transmitter branches are used with two different source signals. The first branch has a PA that suffers from the nonlinear behavior and represents the device under test (DUT), while the second branch has a PA with an ideal linear behavior. Using this setup (two port setup), three signals are available:

- The known input baseband signal, $\boldsymbol{a_1}$, which is inserted to the first PA. The ACLR of input signal, $\boldsymbol{a_1}$, is -62 dBc.
- The coupled input from the 2nd branch, $\boldsymbol{a_2}$, which represents the crosstalk.
- The output, $\boldsymbol{b_2}$, from the first amplifier that has an ACLR of -30 dBc.

The impedance between the PA and the antenna is assumed to be fully matched. Hence, there is no mismatch effect. And there is -1 dB loss between PA and the antenna of each branch. After applying the signals $\boldsymbol{a_1}$ and $\boldsymbol{a_2}$, the output from the first PA, $\boldsymbol{b_2}$ is then registered.

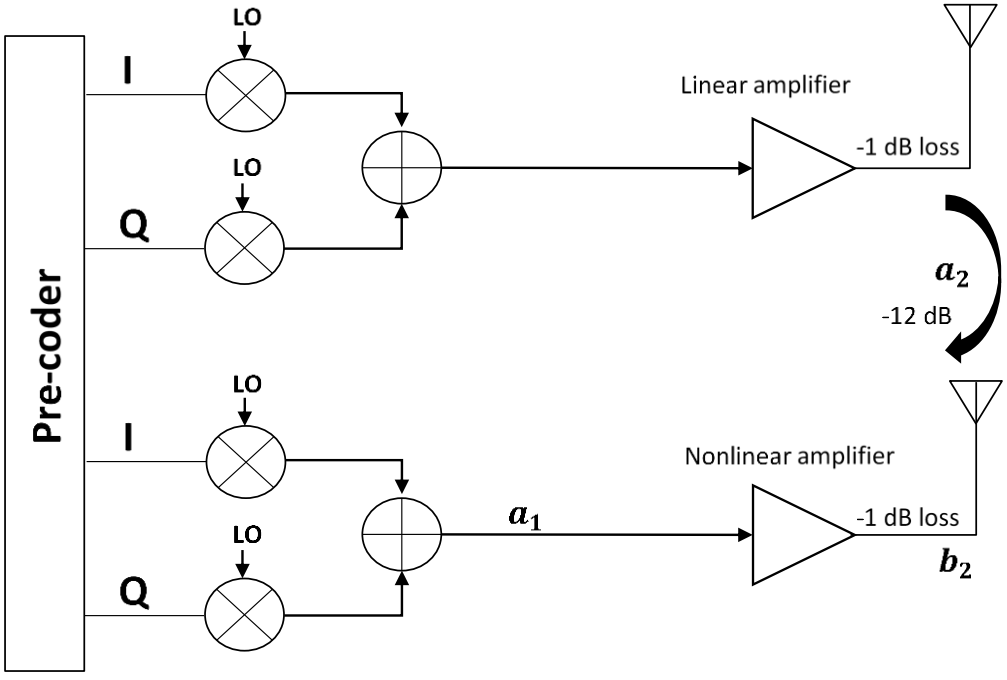

Figure 23: Simulation set-up for model extraction

5.2 Dual-Input PA Model Extraction

To extract the dual-input PA model, (26) is used. In the modeling, first input, $\boldsymbol{a_1}$, second input, $\boldsymbol{a_2}$, and the output, $\boldsymbol{b_2}$, signals are given. These signals are divided into two sets of samples, identification and verification sets. This is done to make sure the modeling using identification set is still valid for the verification set.

To model the PA, a proper selection for memory depths and nonlinear orders is made. To determine the model coefficients $\boldsymbol{\theta_{AMP}}$, the LS method (29) is used. After estimating $\boldsymbol{\theta_{AMP}}$, (26) is used to get the modeled output, $\widehat{\boldsymbol{b}}_{\boldsymbol{2}}$.

In the end, $\boldsymbol{b_2}$ and $\widehat{\boldsymbol{b}}_{\boldsymbol{2}}$ signals should be close. To quantify how they are close, NMSE that measures the model accuracy is used, as illustrated in (31). The NSME threshold is set to be -30 dB. When this condition satisfied, the NMSE of identification set, $NMSE_I$, should be close to the NMSE of verification set, $NMSE_V$, i.e., $NMSE_I \cong NMSE_V$, due to overfitting issue. It is possible to have sub dB difference, otherwise different memory depths and nonlinear orders are selected, as shown in the flowchart in Figure 24.

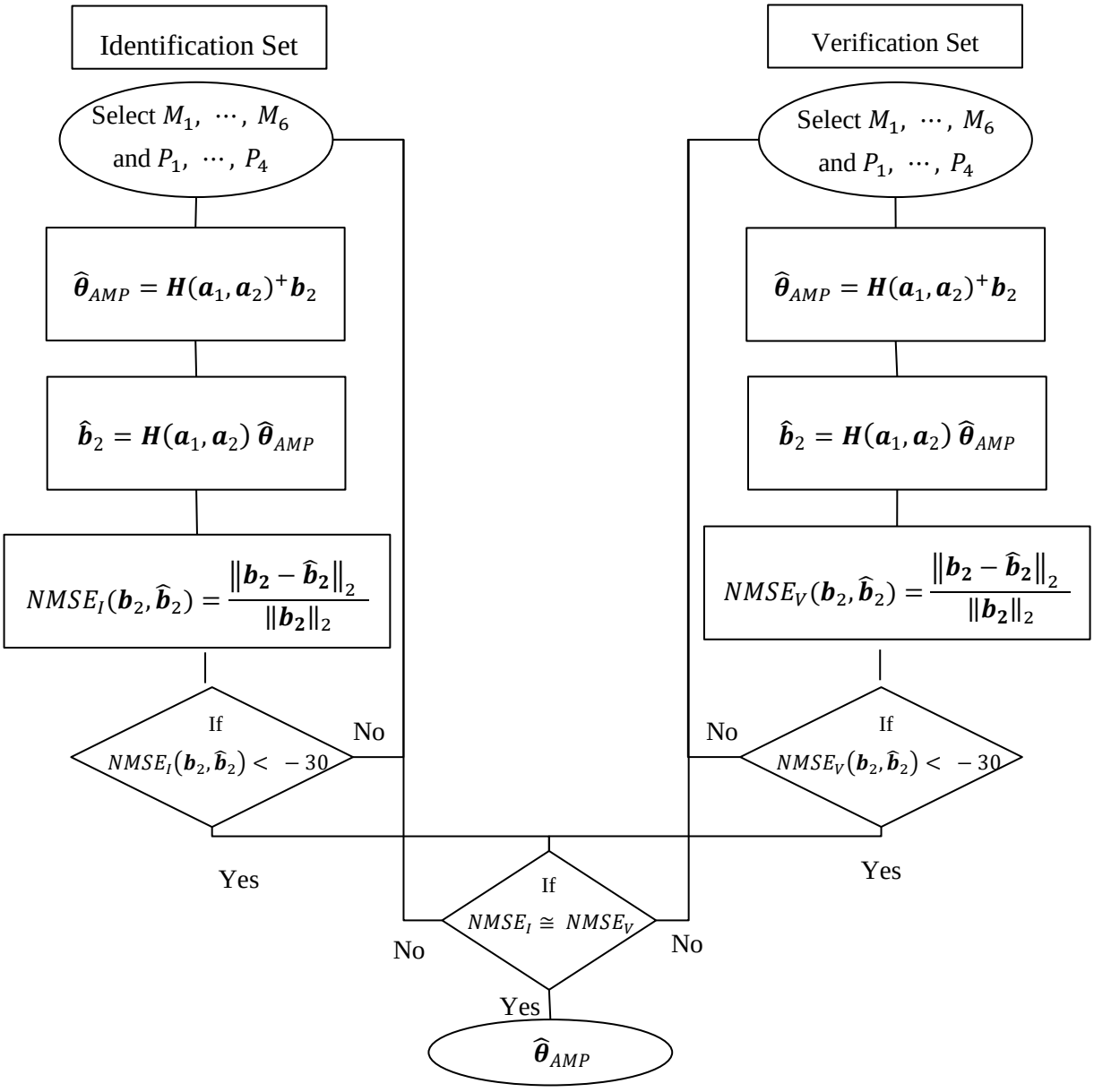

Figure 24: Flowchart of Dual-Input PA Model Extraction

By simulating above flowchart in MATLAB, the model parameters is defined as

- Non-linearity order: P_1=7, P_2=P_3=P_4=5.
- Memory depth: M_1=3, M_2=1, M_3=M_4=M_5=M_6=0.

The resulting NMSE value was around -30 dB.

5.3 Coupling Model

The main goal of this thesis is to relax the isolation level by considering 3GPP requirements, i.e., ACLR=-45 dBc of the amplified signal. To study that, it required to change the coupling level for crosstalk signal, to find the maximum coupling level that corresponds to minimum isolation level. Hence, modeling the coupling is important. One way to change the coupling is by scaling a_2. But we must be careful here as scaling a_2 linearly implies an assumption that the model coefficients will remain same for all values of a_2 which might not be the case in general. The reason is that the a_2 is a nonlinear dependent. Another way to change the coupling is by changing the model coefficients, $\boldsymbol{\theta_{AMP}}$.

To do so, the model coefficients, $\boldsymbol{\theta_{AMP}}$, can be rewritten in terms of $\boldsymbol{\alpha_k}$, $\boldsymbol{\beta_k}$, $\boldsymbol{\gamma_k}$, and $\boldsymbol{\delta_k}$ vectors [17], at k^{th} branch, as shown below,

$$\boldsymbol{\theta_{AMP}} = \left[\boldsymbol{\alpha_k^T}\ \boldsymbol{\beta_k^T}\ \boldsymbol{\gamma_k^T}\ \boldsymbol{\delta_k^T}\right]^{\boldsymbol{T}} \tag{34}$$

Hence, the modeled output signal is redefined as

$$\boldsymbol{b_{2k}} = \boldsymbol{H}(\boldsymbol{a_{1k}}, \boldsymbol{a_{2k}})\left[\boldsymbol{\alpha_k^T}\ \boldsymbol{\beta_k^T}\ \boldsymbol{\gamma_k^T}\ \boldsymbol{\delta_k^T}\right]^{\boldsymbol{T}} \tag{35}$$

To see the impact of changing the coupling level on the modeled output of PA, $\boldsymbol{b_{2k}}$, the model coefficients that corresponds to the $\boldsymbol{a_2}$, i.e., $\boldsymbol{\beta_k}$, $\boldsymbol{\gamma_k}$, and $\boldsymbol{\delta_k}$, are scaled linearly based on coupling level, i.e., multiplying with C_{linear}, as defined below.

$$C_{linear} = 10^{(\boldsymbol{C_{dB}}/20)} \tag{35}$$

5.4 Linearization Gain

One important parameter in linearization algorithm is the linearization gain. This gain, G, is the targeted linear gain for our ILA DPD algorithm. Generally, there are three different types of linearization gain in the literature [24]:

- The linear gain, G_{lin}, is selected when the PA operates in linear region, before the 1dB compression point.

$$G_{lin} = \frac{\underset{\boldsymbol{b_2} \in linear\ region}{max}(|\boldsymbol{b_2}|)}{\underset{\boldsymbol{a_1} \in linear\ region}{max}(|\boldsymbol{a_1}|)} \tag{36}$$

- The peak gain, G_{peak}, is selected when the PA is at maximum power level in both linear and nonlinear regions.

$$G_{peak} = \frac{max(|\boldsymbol{b_2}|)}{max(|\boldsymbol{a_1}|)} \tag{37}$$

- Average gain, G_{Avg}, [24] is calculated so the average power of the output of the pre-distorter is maintained.

$$G_{Avg} = \sqrt{\frac{var(\boldsymbol{b_2})}{var(\boldsymbol{a_1})}} \tag{38}$$

In this thesis, the linear gain, G_{lin}, is used, because DPD performance is better and it converge faster. However, this gain reduces the PA efficiency, by reducing the linearized output power compared to measured one.

5.5 ILA-based MIMO DPD Implementation

For a given input signal, $\boldsymbol{a_1}$, output signal, $\boldsymbol{b_2}$, and the coupling signal, $\boldsymbol{a_2}$, ILA-based MIMO DPD, Figure 25, is implemented to linearize the output, $\boldsymbol{b_2}$. Firstly, the PA is modeled using dual-input MP model, as illustrated earlier in section 5.2. The model parameters of the PA and DPD are assumed to be identical. Then, by scaling the model coefficients, section 5.3, the coupling level is set as an input. The steps for implementing ILA-based MIMO DPD for the dual-input PA model, are summarized as:

- *Step 1)* Estimate PA model coefficients, $\boldsymbol{\theta_{AMP}}$, and set parameters ($M_1, \cdots, M_8$ and $P_1, \cdots, P_4$).
- *Step 2)* Set the desired coupling level by scaling the $\boldsymbol{\beta}^T, \boldsymbol{\gamma}^T$, and $\boldsymbol{\delta}^T$, as stated previously.
- *Step 3*) Set $\boldsymbol{\theta_{DPD}} = [1,0,\cdots,0]^T$.
- *Step 4)* calculate $\boldsymbol{a_{pre}}$, as

$$\boldsymbol{a_{pre}} = \boldsymbol{H}(\boldsymbol{a_1}, \boldsymbol{a_2})\boldsymbol{\theta_{DPD}}$$

- *Step 5*) Calculating the PA output based on PA model coefficients, as

$$\widehat{\boldsymbol{b}}_{\boldsymbol{2}} = \boldsymbol{H}(\boldsymbol{a_{pre}}, \boldsymbol{a_2})\boldsymbol{\theta_{AMP}}$$

- *Step 6)* Normalizing the modeled output, $\widehat{\boldsymbol{b}}_{\boldsymbol{2}}$, by the G_{lin}, as

$$\widehat{\boldsymbol{b}}_{\boldsymbol{2}} = \frac{\widehat{\boldsymbol{b}}_{\boldsymbol{2}}}{G_{lin}}$$

- *Step 7)* Calculate the out-band distortion ACLR for $\widehat{\boldsymbol{b}}_{\boldsymbol{2}}$.
- *Step 8)* If converged, then STOP, else go to step 9.
- *Step 9)* Estimating the post-distorter coefficients, $\widehat{\boldsymbol{\theta}}_{\boldsymbol{DPD}}$, as

$$\widehat{\boldsymbol{\theta}}_{\boldsymbol{DPD}} = \boldsymbol{H}\left(\widehat{\boldsymbol{b}}_{\boldsymbol{2}}, \boldsymbol{a_2}\right)^{+} \boldsymbol{a_{pre}}$$

- *Step 10)* Set the pre-distorter coefficients, $\widehat{\boldsymbol{\theta}}_{\boldsymbol{DPD}}$, to be equal to post-distorter coefficients, $\boldsymbol{\theta_{DPD}}$, as

$$\boldsymbol{\theta_{DPD}} = \widehat{\boldsymbol{\theta}}_{\boldsymbol{DPD}}$$

- *Step 11)* Go to *step 4*.

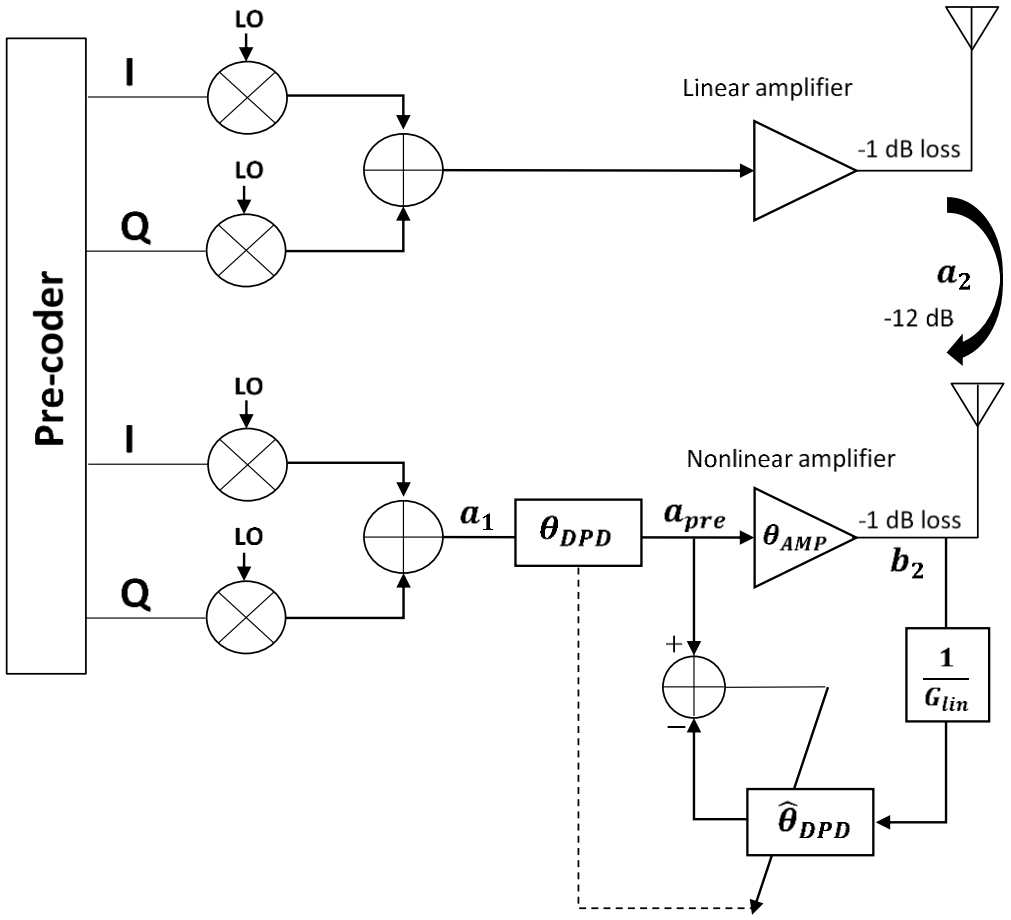

Figure 25 Indirect learning Algorithm with Dual-input PA (MIMO-DPD)

These steps are conducted in MATLAB. The convergence is defined based on the ACLR level, which is set as -45 dBc. But it will not converge if it took more than 5 iterations. The obtained results after simulating these algorithms are presented in the next chapter, where a comparison between MIMO and SISO DPD performance over different levels of coupling will be presented. This comparison will be handled in terms of out and in-band distortions. Furthermore, the performance will also be simulated over different nonlinear orders and memory depths.

6

Results

In this chapter, simulation results are presented for two cases. In first case, there is no crosstalk signal (i.e., no coupling). In second case, there is a coupling of -10 dB. In both cases, SISO and MIMO DPD performance are compared in terms of ACLR, AM/AM, AM/PM, and the power spectrum. Then, SISO and MIMO DPD are applied for different coupling levels, and the resulted ACLR is plotted with respect to different coupling levels. Finally, both model parameters and coupling level are changed to observe the ACLR and set the limits of complexity of MIMO DPD. The complexity is defined in terms of the minimum number of coefficients. These coefficients are selected with respect to 3GPP requirements of -45 dBc ACLR. Additional margin of 5 dBc is added due to the noise from analogue hardware components, hence the targeted ACLR for our system is -50 dBc.

6.1.1 Results without coupling

When no coupling is present between the two antennas, then the SISO DPD and MIMO DPD have the same performance, therefore all the three spectrums (Input, SISO and MIMO DPD outputs) are overlapped on top of each other, as in Figure 26. All the signals are normalized to easily be compared with the input signal. Measured output represents the PA output without DPD.

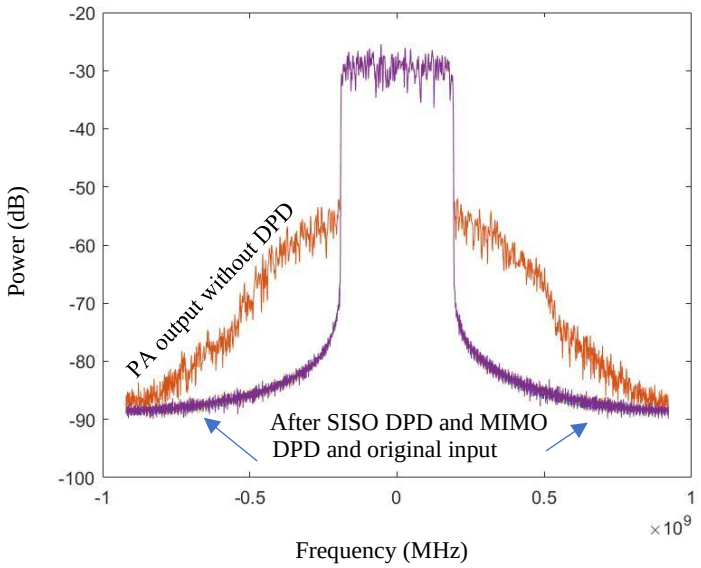

Figure 26: Input and Output spectrum without coupling

Again, when no coupling is introduced, MIMO and SISO DPD have the same performance as appears in AM/AM Figure 27 and Figure 28, AM/PM Figure 29 and Figure 30.

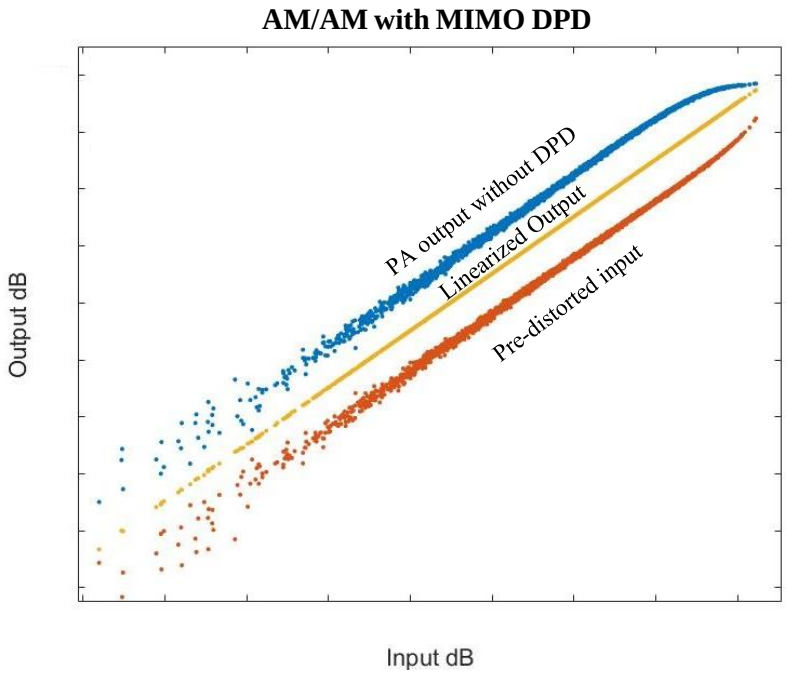

Figure 27: AM/AM MIMO without coupling

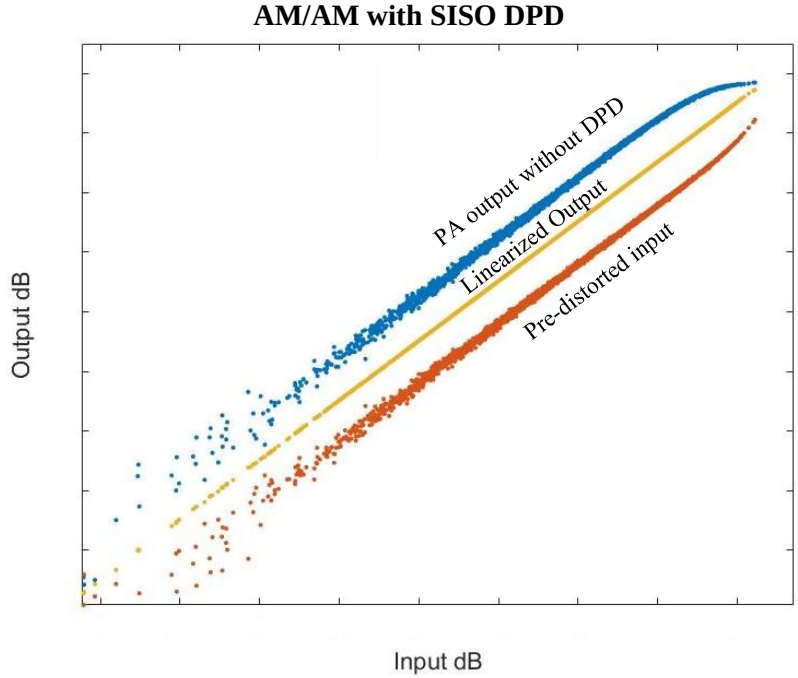

Figure 28: AM/AM SISO without coupling

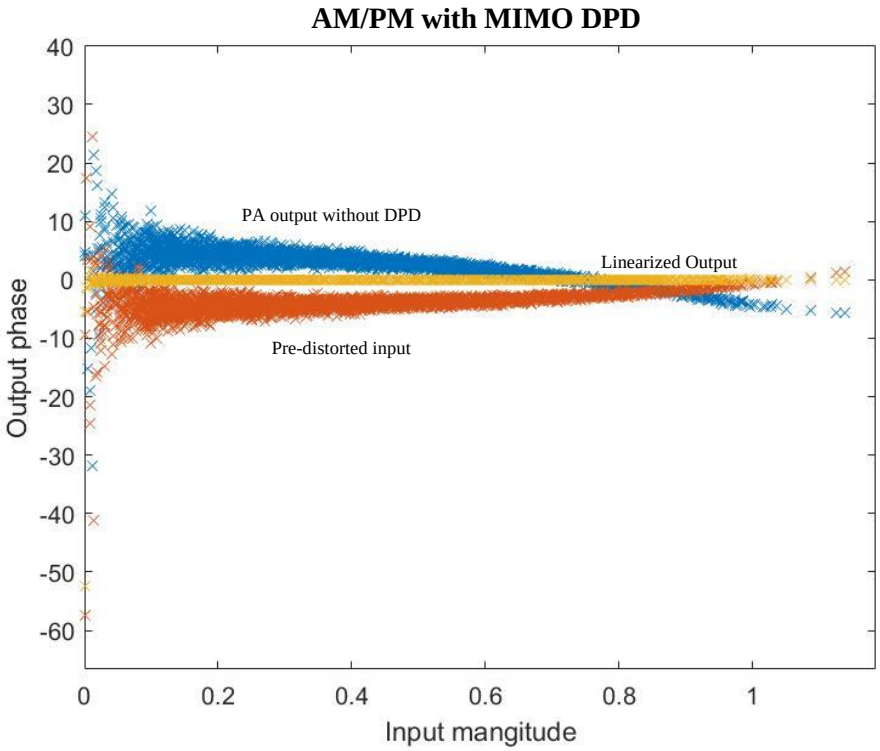

Figure 29: AM/PM MIMO without coupling

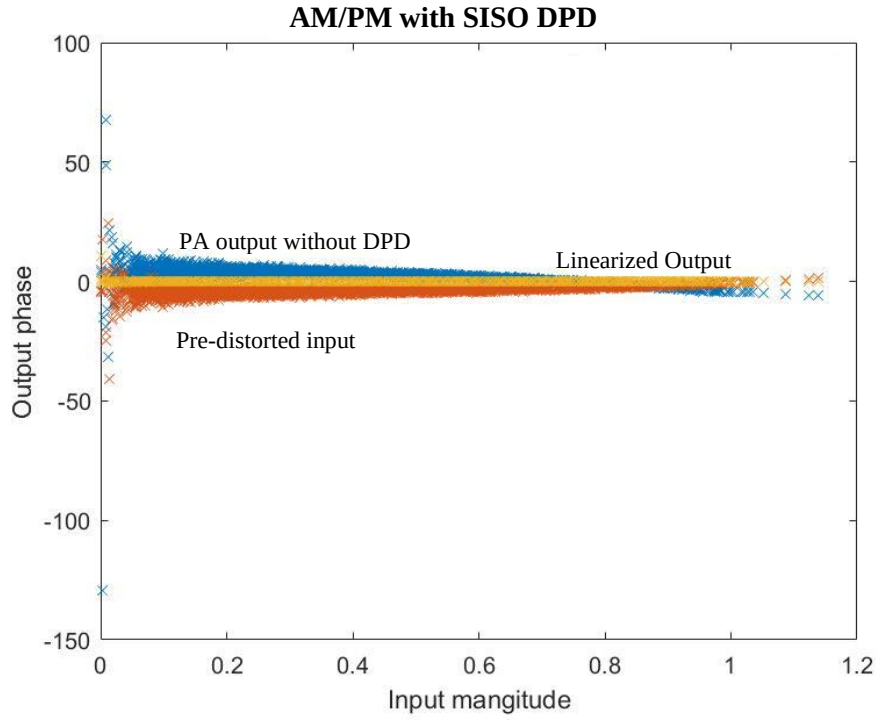

Figure 30: AM/PM SISO without coupling

In case of no coupling, both SISO and MIMO DPD have similar performance. The reason is that the contributions from the coupling input is almost none. Hence, it is not required to use MIMO DPD

in this case. However, with MIMO systems, the coupling is always existing. For this reason, the coupling is important to be considered, as explained next.

6.1.2 Results with coupling

In this case, the crosstalk signal is introduced to the PA with coupling level of -10 dB. Hence, the nonlinear distortion behavior is changed. To model the impact of this coupling on the PA behavior, the model coefficients that corresponds to the crosstalk signal, i.e., $\boldsymbol{\beta_k}$, $\boldsymbol{\gamma_k}$, and $\boldsymbol{\delta_k}$, are scaled linearly based on coupling level, as explained in section 5.3. After using DPD to linearize PA performance, the MIMO DPD has a better performance than SISO DPD, as shown in Figure 31. MIMO DPD almost compensates for all nonlinear distortions; hence, the output is a linear amplified version of its input. Meanwhile, SISO DPD can't compensate for coupling signal.

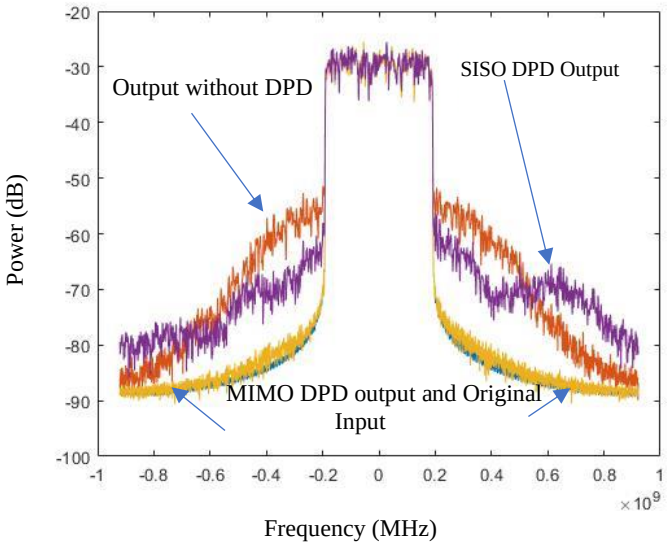

Figure 31: Input and Output spectrum with coupling

In high coupling level, SISO DPD presents higher distortion in the linearized output which appears as a yellow cloud in Figure 32, while MIMO DPD gives a linearized output that appears as a yellow sharp line in Figure 33.

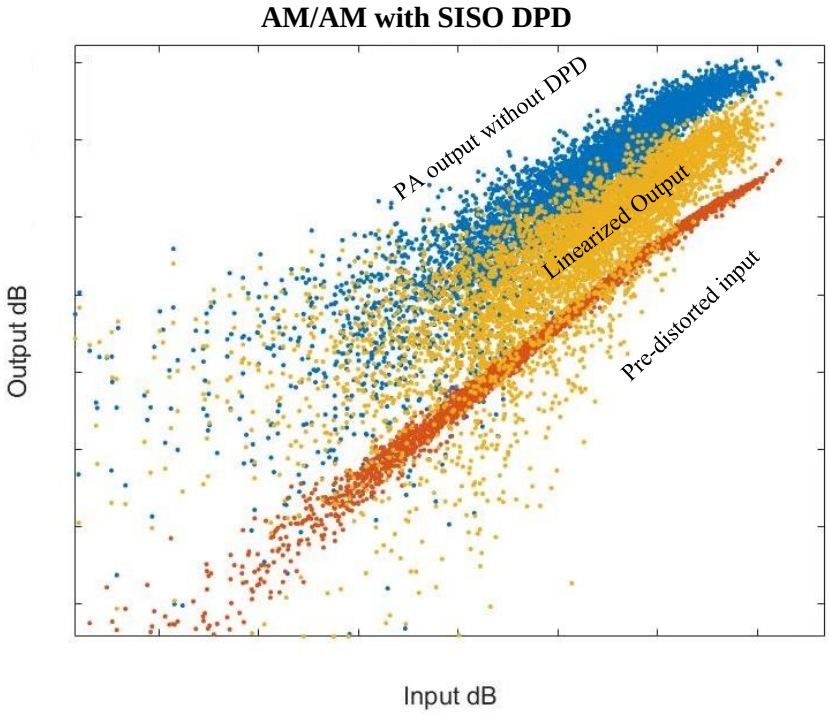

Figure 32: AM/AM SISO with coupling

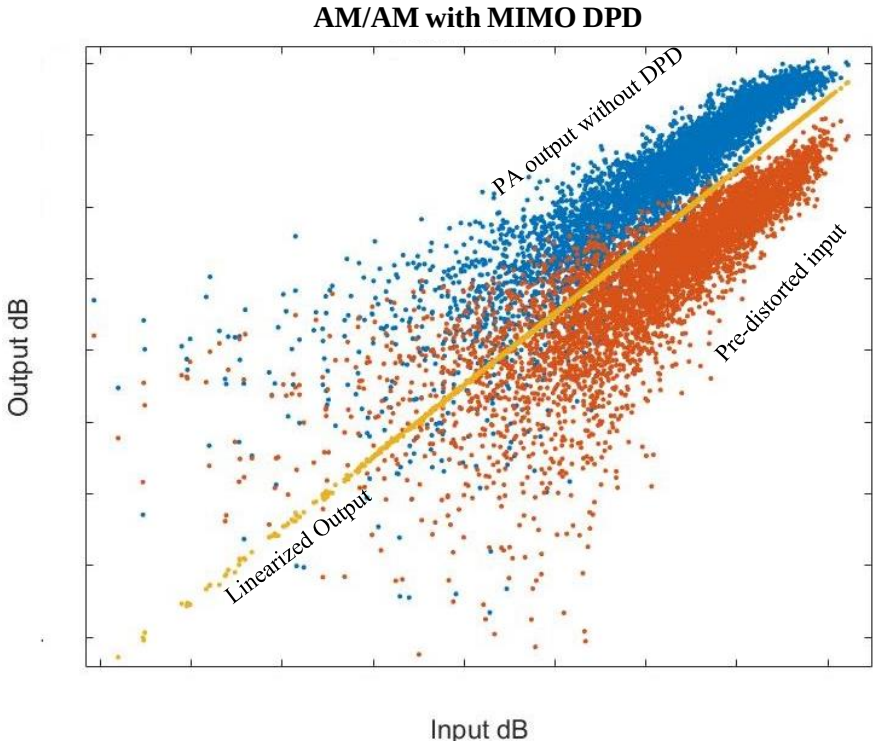

Figure 33: AM/AM MIMO with coupling

The same conclusion can be generalized for the AM-PM in Figure 34 and Figure 35.

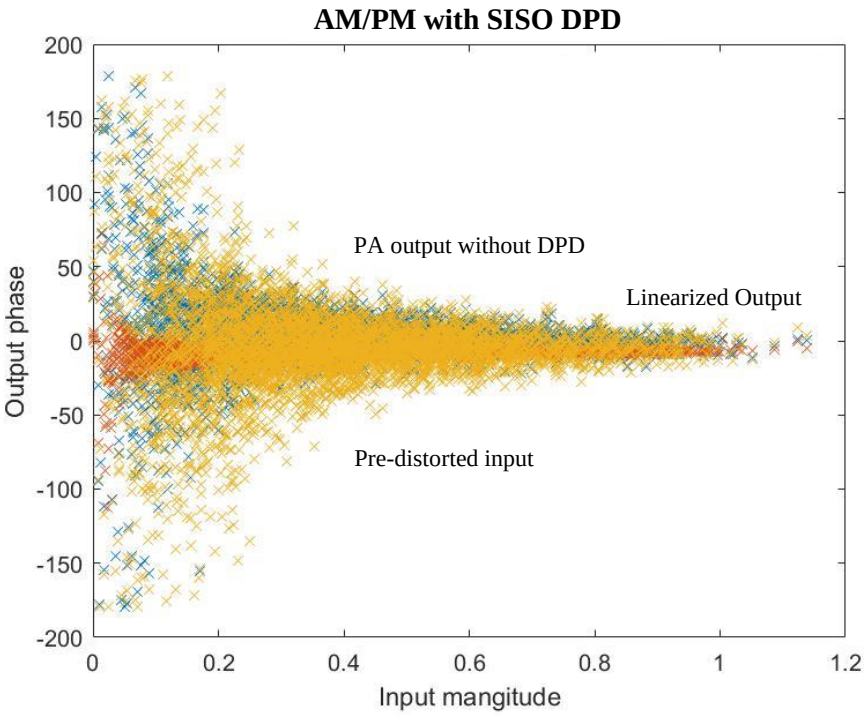

Figure 34: AM-PM SISO with coupling

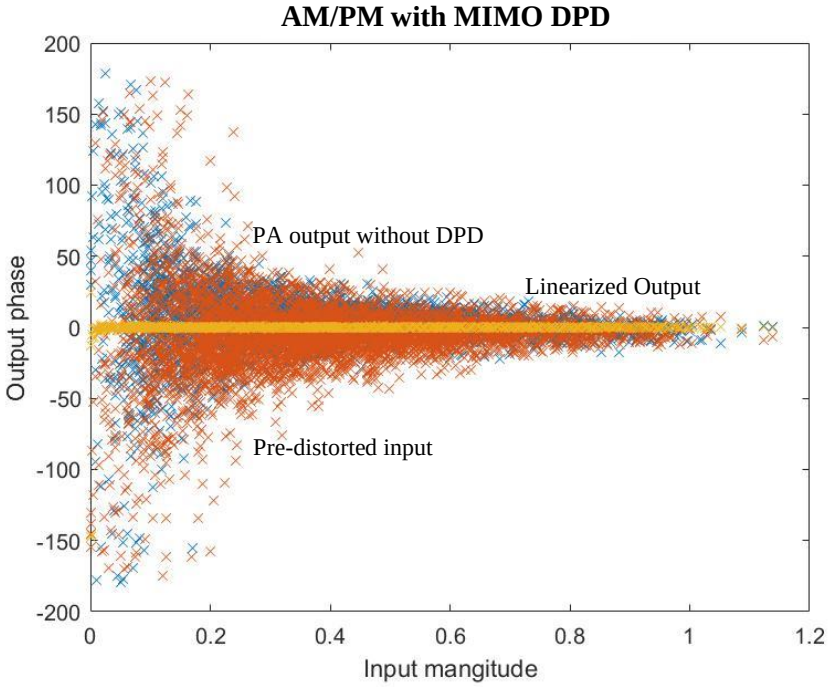

Figure 35: AM-PM MIMO with coupling

A relationship between the coupling and the ACLR, is illustrated in Figure 36. It can be seen that, to achieve the targeted ACLR requirements, i.e., -50 dB ACLR, the isolation can be relaxed to make the coupling level of -11 dB.

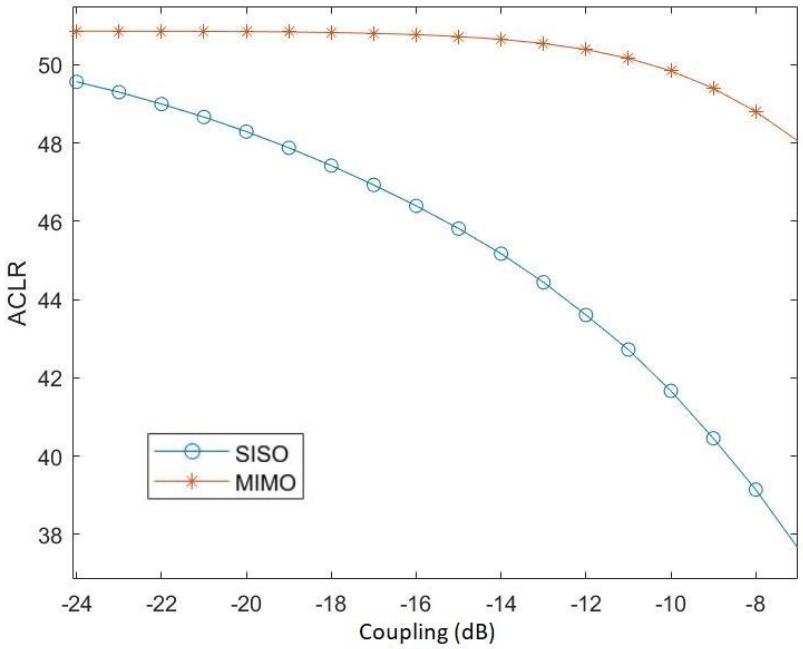

Figure 36: Coupling vs. ACLR

In-band distortion is more sensitive to changes in coupling than the out-of-band distortion. However, MIMO DPD is more stable than the SISO DPD as it can be seen from Figure 37.

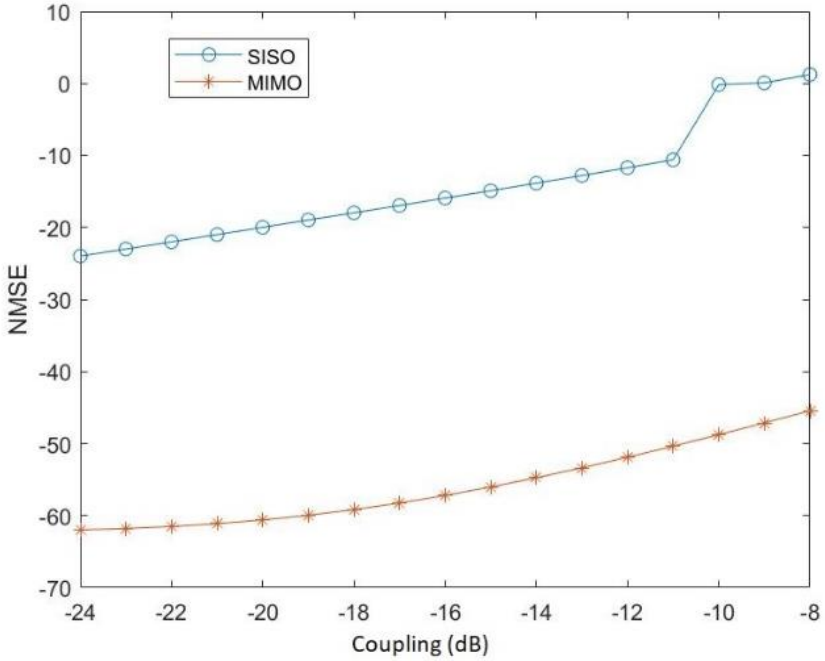

Figure 37: Coupling vs. NMSE

Another study is made by changing the PA model in terms of memory depth and non-linear order, with changing of coupling level as in Figure 38. It has been seen the model accuracy (NMSE) is better when increasing the memory depth and nonlinearity order but the enhancement for ACLR is increased by sub dB, so it is sufficient to choose nonlinear order 5.

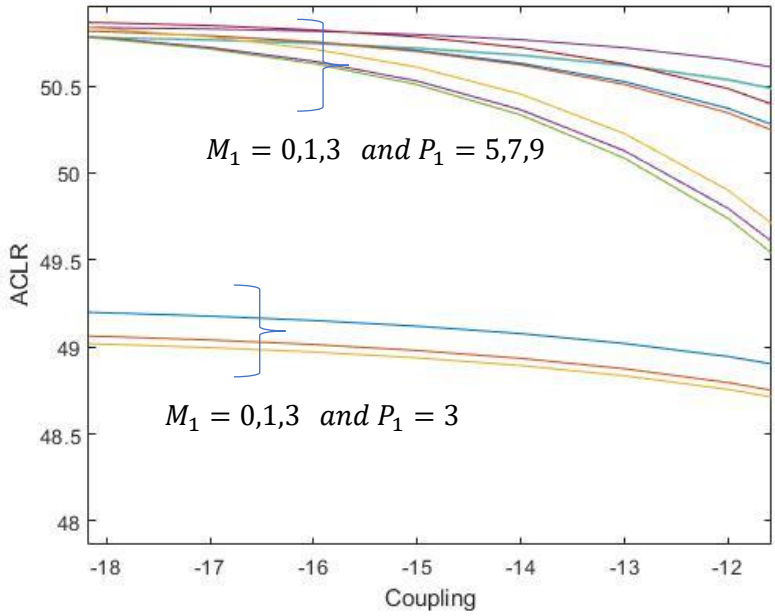

Figure 38: Coupling vs. ACLR vs. Memory Depth and Nonlinear Order

7

Conclusion and Future Work

7.1 Conclusion

This project report presented challenging issues in modern radio communication systems related to nonlinearities of PAs, which is introduced by PA itself and crosstalk from other branches. It also illustrates how these effects can be modelled using Dual-input Memory Polynomial after suitable selection for memory depths and nonlinear orders. These selections are done with respect to NMSE level. After modeling the PA and estimating the model coefficients, the PA behavioral model is pre-inversed using pre-distorter before PA. A digital pre-distortion method using the ILA is used to estimate the pre-distorter coefficients in iterative closed-loop way.

In case of full isolation, SISO DPD and MIMO DPD give similar performance in terms of ACLR (out-of-band distortion) and NMSE (in-band distortion). When there is coupling level of -10 MIMO DPD has better performance than SISO DPD, because it compensates for 2nd crosstalk coupling signal.

By changing the coupling level, the ACLR after using MIMO DPD has lower level than the one after using SISO DPD, as well as the NMSE level for MIMO DPD is better. In case of higher complex model, when the nonlinear order is higher than 5, there is no improvement in the DPD performance in terms of ACLR. It can be concluded that by using the proposed linearization method, the isolation level can be relaxed by at least a 11 dB while preserving the targeted ACLR level of -50 dB with nonlinear order 5.

7.2 Future Work

After investigating the proposed DPD considering only two branches, the ongoing process is to simulate the whole AAS system, Figure 39, (128×128 dual polarized antenna array) considering coupling and mismatch effects from different adjacent branches and for different polarization (vertical and horizontal). The proposed method for multiple branches which was illustrated in section 3.4 can be applied.

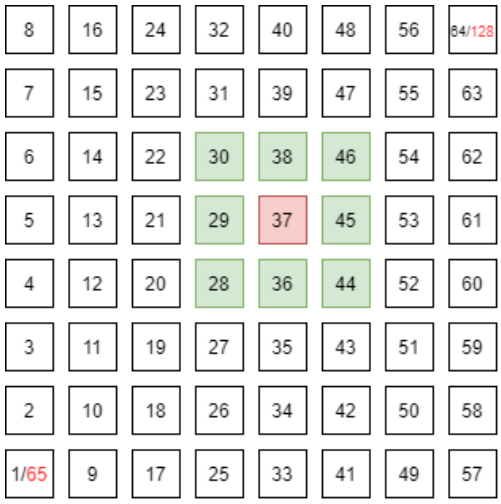

Figure 39: 128×128 Dual Polarized Antenna Array

Furthermore, after succeeding in implementing the DPD using ILA technique, a step forward to implement the Iterative Learning Control (ILC) may be also considered to achieve better performance even with the stronger PA non-linearity.

8

References

[1] D. M. Pozar, *Microwave and RF Design of Wireless Systems*, John Wiley & Sons, Inc., 2001.

[2] Andrae, Anders & Edler, Tomas. (2015). On Global Electricity Usage of Communication Technology: Trends to 2030. Challenges. 6. 117-157. 10.3390/challe6010117..

[3] I. Humar, X. Ge, L. Xiang, M. Jo, M. Chen and J. Zhang, "Rethinking energy efficiency models of cellular networks with embodied energy," in IEEE Network, vol. 25, no. 2, pp. 40-49, March-April 2011. doi: 10.1109/MNET.2011.5730527.

[4] S. M. Razavizadeh, M. Ahn and I. Lee, "Three-Dimensional Beamforming: A new enabling technology for 5G wireless networks," in IEEE Signal Processing Magazine, vol. 31, no. 6, pp. 94-101, Nov. 2014. doi: 10.1109/MSP.2014.2335236.

[5] M. K. Kazimierczuk, *RF Power Amplifiers*, Wileys, 2015.

[6] P.-S. Kildal, *Foundations of Antenna Engineering: A Unified Approach for Line-of-Sight and Multipath*, Gothenburg, Sweden: Kildal Antenn AB, 2015.

[7] E. Bjornson, L. Van der Perre, S. Buzzi and E. G. Larsson, "Massive MIMO in Sub-6 GHz and mmWave: Physical, Practical, and Use-Case Differences," in IEEE Wireless Communications, vol. 26, no. 2, pp. 100-108, April 2019. doi: 10.1109/MWC.2018.1800140

[8] M. S. e. al., “Linearly Polarized 64-element Antenna Array for mm-Wave Mobile Backhaul Application,” *European Conference on Antennas and Propagation*, London, 2018.

[9] I. Agilent Technologies, “4G MIMO ANTENNA DESIGN AND VERIFICATION,” 2008. [Online]. Available: https://www.keysight.com/upload/cmc_upload/All/Antenna-Design-GENESYS_ver4.pdf. [Accessed 14 6 2019].

[10] I. Rosu. [Online]. Available: https://www.qsl.net/va3iul/RF%20Power%20Amplifiers/RF_Power_Amplifiers.pdf. [Accessed 14 6 2019].

[11] M. Yarleque, *RF Power Amplifiers for Wireless Communication*, Leuven (Heverlee), België, June, 2008.

[12] D. M. Pozar, *Microwave Engineering*, 2005.

[13] Gregorio, Fernando & Cousseau, Juan & Werner, Stefan & Riihonen, Taneli & Wichman, Risto. (2011). Power amplifier linearization technique with IQ imbalance and crosstalk compensation for broadband MIMO-OFDM transmitters. Eurasip Journal on Advances in Signal Processing - EURASIP J ADV SIGNAL PROCESS. 2011. 1-15. 10.1186/1687-6180-2011-19.

[14] X. Bland, "Modeling of Power Amplifier Distortion in MIMO Transmitters," *Chalmers University of Technology*, Gothenburg, Sweden, 2013.

[15] J. Vuolevi T. Rahkonen , *Distortion in RF power amplifiers*, Norwood, ARTECH HOUSE, INC., 2003.

[16] K. Hausmair, "Modeling and Compensation of Nonlinear Distortion in Multi-Antenna RF Transmitters," *Chalmers University of Technology*, Gothenburg, Sweden, 2018.

[17] Hoi-Shun Lui, H. T. Hui and Mook Seng Leong, "A Note on the Mutual-Coupling Problems in Transmitting and Receiving Antenna Arrays," in IEEE Antennas and Propagation Magazine, vol. 51, no. 5, pp. 171-176, Oct. 2009. doi: 10.1109/MAP.2009.5432083

[18] D. Nopchinda and K. Buisman, "Measurement Technique to Emulate Signal Coupling Between Power Amplifiers," in IEEE Transactions on Microwave Theory and Techniques, vol. 66, no. 4, pp. 2034-2046, April 2018. doi: 10.1109/TMTT.2017.2786274

[19] S. Goyel, J. Gupta, "Review Of Power Amplifier Linearization Techniques In Communication System," *International Journal of Engineering Research & Technology (IJERT)*, vol. 2, no. 6, pp. 1897-1904, June - 2013.

[20] J. Chani-Cahuana, P. N. Landin, C. Fager and T. Eriksson, "Iterative Learning Control for RF Power Amplifier Linearization," in IEEE Transactions on Microwave Theory and Techniques, vol. 64, no. 9, pp. 2778-2789, Sept. 2016. doi: 10.1109/TMTT.2016.2588483

[21] D. A. Bristow, M. Tharayil and A. G. Alleyne, "A survey of iterative learning control," in IEEE Control Systems Magazine, vol. 26, no. 3, pp. 96-114, June 2006. doi: 10.1109/MCS.2006.1636313

[22] P. N. Landin, A. E. Mayer and T. Eriksson, "MILA - A noise mitigation technique for RF power amplifier linearization," 2014 IEEE 11th International Multi-Conference on Systems, Signals & Devices (SSD14), Barcelona, 2014, pp. 1-4. doi: 10.1109/SSD.2014.6808874

[23] H. Paaso and A. Mammela, "Comparison of direct learning and indirect learning predistortion architectures," 2008 IEEE International Symposium on Wireless Communication Systems, Reykjavik, 2008, pp. 309-313. doi: 10.1109/ISWCS.2008.4726067

[24] S. Wang, M. A. Hussein, O. Venard and G. Baudoin, "Impact of the normalization gain of digital predistortion on linearization performance and power added efficiency of the linearized power amplifier," 2017 47th European Microwave Conference (EuMC), Nuremberg, 2017, pp. 1050-1053. doi: 10.23919/EuMC.2017.8231026

[25] "Meca Electronics Inc," Microwave Equipments and Components of America, [Online]. Available: http://www.e-meca.com/. [Accessed 10 May 2019].

[26] https://www.3gpp.org/news-events/1929-nsa_nr_5g

[27] K. Hausmair, P. N. Landin, U. Gustavsson, C. Fager and T. Eriksson, "Digital Predistortion for Multi-Antenna Transmitters Affected by Antenna Crosstalk," in IEEE Transactions on Microwave Theory and Techniques, vol. 66, no. 3, pp. 1524-1535, March 2018. doi: 10.1109/TMTT.2017.2748948

[28] P. N. Landin, M. Isaksson, and P. H¨andel, “Parameter extractionand performance evaluation method for increased performance in RFpower amplifier behavioral modeling,”Int. Journal of RF and Microw.Computer-Aided Engineering, vol. 20, no. 2, pp. 200–208, 2010. [Online].Available: http://dx.doi.org/10.1002/mmce.20422

[29] J. Chani-Cahuana, P. N. Landin, C. Fager and T. Eriksson, "Iterative Learning Control for RF Power Amplifier Linearization," in IEEE Transactions on Microwave Theory and Techniques, vol. 64, no. 9, pp. 2778-2789, Sept. 2016. doi: 10.1109/TMTT.2016.2588483

9

Appendices

9.1 Notations in this report

In this thesis, the incidence wave to the PA is represented by $\boldsymbol{a_1}$ while the coupling input is represented by $\boldsymbol{a_2}$, which is the back-coming incident voltage wave due to coupling and mismatch, and $\boldsymbol{b_2}$ is the scattered voltage wave (the output) from the PA, Figure 40.

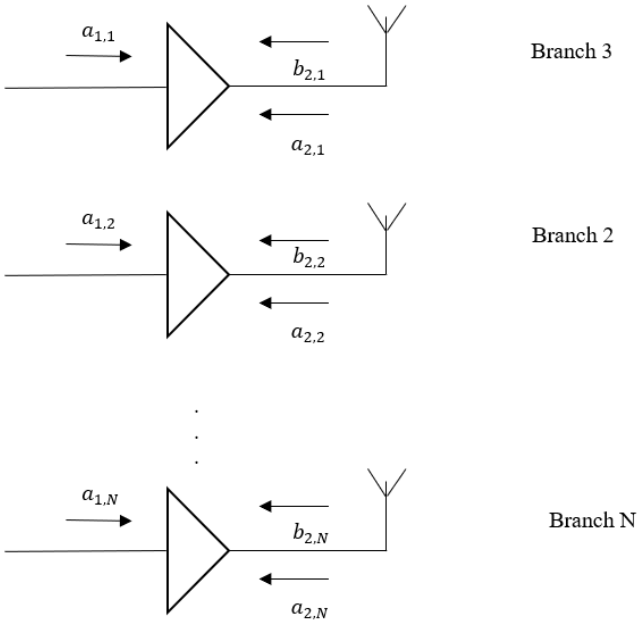

Figure 40: N×N MIMO transmitter [17]

9.2 Circulators and Isolators

A circulator, Figure 41 and Figure 42 (a), is a three port microwave device that can be lossless and matched at all ports. The scattering matrix of an ideal three-port circulator can be written as:

$$[S] = \begin{bmatrix} 0 & 0 & 1 \\ 1 & 0 & 0 \\ 0 & 1 & 0 \end{bmatrix}$$

This means that the power can follow from port one to port two, from port two to port three and from port three to port three but no power flows in the reverse directions [12].

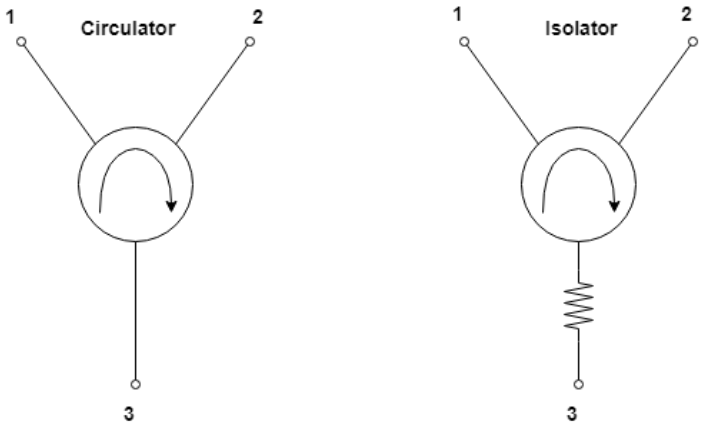

Figure 41: Circulator and Isolator block diagram

In Figure 41 and Figure 42 (b), port 1 is terminated to make sure that any reflected signal in port 2 will totally be absorbed by the resistor in the third port and nothing of this reflected wave will pass through port 1 again. The isolator is then used to isolate the device under test from any type of unwanted reflection that may affect it is performance.

(a)

(b)

Figure 42: Physical devices (a): Circulator, (b): Isolator.